

Predictions for $p+\text{Pb}$ Collisions at $\sqrt{s_{NN}} = 5 \text{ TeV}$: Expectations vs. Data

R. Vogt

Lawrence Livermore National Laboratory, Livermore, CA 94551, USA
Physics Department, University of California, Davis, CA 95616, USA

with members and friends of the JET Collaboration

From Int. J. Mod. Phys. E 22 (2013) 1330007 [arXiv:1301.3395 [hep-ph]]

Contributions from: Javier Albacete *et al.* (rcBK, charged hadrons), Nestor Armesto (jets), Kari Eskola (π^0), Rainer Fries (direct photons), Vasile Topor Pop *et al.* (HIJINGBB), Boris Kopeliovich ($R_{p\text{Pb}}$), Kryzstof Kutak (azimuthal difference between jets), Gergeley Barnafoldi *et al.* (charged hadrons, forward/backward asymmetry), Rudolf Baier *et al.* (forward photons and dileptons), Amir Rezaeian (b-CGC charged hadrons, rcBK photons), Ivan Vitev (charged hadrons, π^0 , photons), Xin-Nian Wang (charged hadrons), Jianwei Qiu (gauge bosons), Ben-Wei Zhang (jets, gauge bosons), Ziwei Lin (AMPT), Raju Venugopalan *et al.* (IP-Sat), RV (J/ψ), Francois Arleo (J/ψ)

Outline

We stick to results where data are already available

Model descriptions are combined with available data

- Charged particles

- $dN_{\text{ch}}/d\eta$

- dN_{ch}/dp_T

- $R_{p\text{Pb}}(p_T)$

- J/ψ

- $R_{p\text{Pb}}(y)$

- $R_{F/B}(y), R_{F/B}(p_T)$

Model Descriptions

Saturation

Saturation: rcBK (A. Rezaeian, J. Albacete *et al*)

Gluon jet production in pA described by k_T -factorization

$$\frac{d\sigma}{dy d^2p_T} = \frac{2\alpha_s}{C_F} \frac{1}{p_T^2} \int d^2\vec{k}_T \phi_p^G(x_1; \vec{k}_T) \phi_A^G(x_2; \vec{p}_T - \vec{k}_T)$$

Here $x_{1,2} = (p_T/\sqrt{s})e^{\pm y}$ and unintegrated gluon density, $\phi_A^G(x_i; \vec{k}_T)$, is related to color dipole forward scattering amplitude

$$\begin{aligned} \phi_A^G(x_i; \vec{k}_T) &= \frac{1}{\alpha_s} \frac{C_F}{(2\pi)^3} \int d^2\vec{b}_T d^2\vec{r}_T e^{i\vec{k}_T \cdot \vec{r}_T} \nabla_T^2 \mathcal{N}_A(x_i; r_T; b_T) \\ \mathcal{N}_A(x_i; r_T; b_T) &= 2\mathcal{N}_F(x_i; r_T; b_T) - \mathcal{N}_F^2(x_i; r_T; b_T) \end{aligned}$$

In k_T -factorized approach, both projectile and target have to be at small x so that CGC formalism is applicable to both

rcBK Hybrid Approach

Hybrid models that treat the projectile (forward) with DGLAP collinear factorization and target with CGC methods

Hadron cross section is proportional to $f_g(x_1, \mu_F^2)N_A(x_2, p_T/z) + f_q(x_1, \mu_F^2)N_F(x_2, p_T/z)$ modulo fragmentation functions

$$\begin{aligned} \frac{dN^{pA \rightarrow hX}}{d\eta d^2p_T} &= \frac{K}{(2\pi)^2} \left[\int_{x_F}^1 \frac{dz}{z^2} \left[x_1 f_g(x_1, \mu_F^2) N_A(x_2, \frac{p_T}{z}) D_{h/g}(z, \mu_{Fr}) \right. \right. \\ &+ \left. \Sigma_q x_1 f_q(x_1, \mu_F^2) N_F(x_2, \frac{p_T}{z}) D_{h/q}(z, \mu_{Fr}) \right] \\ &+ \frac{\alpha_s^{\text{in}}}{2\pi^2} \int_{x_F}^1 \frac{dz}{z^2} \frac{z^4}{p_T^4} \int_{k_T^2 < \mu_F^2} d^2k_T k_T^2 N_F(k_T, x_2) \int_{x_1}^1 \frac{d\xi}{\xi} \\ &\times \left. \Sigma_{i,j=q,\bar{q},g} w_{i/j}(\xi) P_{i/j}(\xi) x_1 f_j(\frac{x_1}{\xi}, \mu_F) D_{h/i}(z, \mu_{Fr}) \right]. \end{aligned}$$

K factor introduced to incorporate higher order corrections

Inelastic term is multiplied by α_s^{in} , different from running α_s in rcBK equation – in hybrid formulation, strong coupling in dilute regime (proton) can differ from that in the dense system (nucleus) but appropriate scale of α_s^{in} cannot be determined without a NNLO calculation

Factorization, renormalization and fragmentation scales assumed to be equal, $\mu_F = \mu_R = \mu_{Fr}$ with $\mu_F = 2p_T$, p_T and $p_T/2$ to form uncertainty range for given N and α_s^{in}

rcBK Equation

$N_{A(F)}$ is 2-D Fourier transform of imaginary part of dipole scattering amplitude in the fundamental (F) or adjoint (A) representation $\mathcal{N}_{A(F)}$

$\mathcal{N}_{A(F)}$ calculated using JIMWLK which simplifies to BK in the large N_c limit

Running coupling corrections to LL kernel result in rcBK equation

$$\frac{\partial \mathcal{N}_{A(F)}(r, x)}{\partial \ln(x_0/x)} = \int d^2 \vec{r}_1 K^{\text{run}}(\vec{r}, \vec{r}_1, \vec{r}_2) [\mathcal{N}_{A(F)}(r_1, x) + \mathcal{N}_{A(F)}(r_2, x) - \mathcal{N}_{A(F)}(r, x) - \mathcal{N}_{A(F)}(r_1, x) \mathcal{N}_{A(F)}(r_2, x)]$$

$$\mathcal{N}(r, Y=0) = 1 - \exp \left[-\frac{(r^2 Q_{0s}^2)^\gamma}{4} \ln \left(\frac{1}{\Lambda r} + e \right) \right]$$

Last equation is initial condition with γ fixed from DIS data, $\gamma = 1$ is MV initial condition, $\gamma \sim 1.1$ in fits

$Q_{0p}^2 \sim 0.2 \text{ GeV}^2$ in MV initial condition, smaller for other values of γ

$Q_{0A}^2 \sim N Q_{0p}^2$ with $3 < N < 7$ in Rezaeian's calculations, Albacete *et al* let nuclear scale be proportional to the number of participants at a given b to account for geometrical fluctuations in Monte Carlo simulations

Saturation: IP-Sat (Triebedy and Venugopalan)

Here one starts as before with k_T -factorization

$$\frac{dN_g^{pA}(b_T)}{dy d^2p_T} = \frac{4\alpha_s}{\pi C_F} \frac{1}{p_T^2} \int \frac{d^2k_T}{(2\pi)^5} \int d^2s_T \frac{d\phi_p(x_1, k_T|s_T)}{d^2s_T} \frac{d\phi_A(x_2, p_T - k_T|s_T - b_T)}{d^2s_T}$$

Unintegrated gluon density is expressed in terms of the dipole cross section as

$$\frac{d\phi^{p,A}(x, k_T|s_T)}{d^2s_T} = \frac{k_T^2 N_c}{4\alpha_s} \int_0^\infty d^2r_T e^{i\vec{k}_T \cdot \vec{r}_T} \left[1 - \frac{1}{2} \frac{d\sigma_{\text{dip}}^{p,A}}{d^2s_T}(r_T, x, s_T) \right]^2$$

Dipole cross section is a refinement of Golec-Biernat–Wusthoff that gives the right perturbative limit for $r_T \rightarrow 0$, equivalent to effective theory of CGC to LL

$$\frac{d\sigma_{\text{dip}}^p}{d^2b_T}(r_T, x, b_T) = 2 \left[1 - \exp \left(-\frac{\pi^2}{2N_c} r_T^2 \alpha_s(\mu^2) x g(x, \mu^2) T_p(b_T) \right) \right]$$

μ^2 is related to dipole radius, r_T , by $\mu^2 = \frac{4}{r_T^2} + \mu_0^2$

The gluon density $g(x, \mu^2)$ is LO DGLAP result without quarks

$T_p(b_T)$ is the gluon density profile function, $T_p(b_T) = (2\pi B_G)^{-1} \exp[-(b_T^2/2B_G)]$ where $\langle b^2 \rangle = 2B_G$, the average squared gluonic radius of the proton, obtained from HERA data

Event-by-Event Calculations

HIJING2.0 (X.-N. Wang *et al*)

Based on two-component model of hadron production, soft (string excitations with effective cross section σ_{soft}) and hard (perturbative QCD) components separated by cutoff momentum p_0

LO pQCD calculation with K factor to absorb higher-order corrections

$$\frac{d\sigma_{pA}^{\text{jet}}}{dy_1 d^2p_T} = K \int dy_2 d^2b T_A(b) \sum_{a,b,c} x_1 f_{a/p}(x_1, p_T^2) x_2 f_{a/A}(x_2, p_T^2, b) \frac{d\sigma_{ab \rightarrow cd}}{dt}$$

Effective $2 \rightarrow 2$ scattering, $x_{1,2} = p_T(e^{\pm y_1} + e^{\pm y_2})/\sqrt{s}$

Default HIJING collisions decomposed into independent and sequential NN collisions – in each NN interaction, hard collisions simulated first, followed by soft

Since hard interactions occur over shorter time scale, HIJING2.0 also uses decoherent hard scattering (DHC) where all hard collisions are simulated first, then soft, so available energy unrestricted by soft interactions

Energy-dependent k_T broadening in HIJING

$$\langle k_T^2 \rangle = [0.14 \log(\sqrt{s}/\text{GeV}) - 0.43] \text{ GeV}^2/c^2$$

Shadowing in HIJING

Shadowing treated as scale independent

Versions before HIJING2.0 did not differentiate between quark and gluon shadowing

$$\begin{aligned}f_{a/A}(x, \mu_F^2, b) &= S_{a/A}(x, \mu_F^2, b) f_{a/A}(x, \mu_F^2) \\S_{a/A}(x) &\equiv \frac{f_{a/A}(x)}{A f_{a/N}(x)} \\&= 1 + 1.19 \log^{1/6} A [x^3 - 1.2x^2 + 0.21x] \\&\quad - s_a (A^{1/3} - 1)^n \left[1 - \frac{10.8}{\log(A+1)} \sqrt{x} \right] e^{-x^2/0.01} \\s_a(b) &= s_a \frac{5}{3} \left(1 - \frac{b^2}{R_A^2} \right)\end{aligned}$$

In HIJING2.0 the $(A^{1/3} - 1)$ factor is nonlinear ($n = 0.6$) but $n = 1$ in earlier versions

Previously $s_a = s_g = s_q = 0.1$

In HIJING2.0 $s_g \neq s_q$: $s_q = 0.1$ and $s_g \sim 0.22 - 0.23$ to match LHC data

The b dependence of s_a gives some impact parameter dependence to $S_{a/A}$

HIJINGB \bar{B} (V. Topor Pop *et al*)

Differs from standard HIJING in treatment of fragmentation

HIJING uses string fragmentation with constant vacuum value of $\kappa_0 = 1.0 \text{ GeV/fm}$ for string tension

HIJINGB \bar{B} allows for multiple overlapping flux tubes leading to strong longitudinal color field (SCF) effects

SCF effects modeled by varying κ and momentum cutoff with \sqrt{s} and A

Fragmentation also modified, including baryon loops to explain baryon to meson anomaly and increase strange baryon production

AMPT: A Multi-Phase Transport (Z. Lin)

AMPT is a Monte Carlo transport model for heavy ion collisions, montage of other codes

- Heavy Ion Jet Interaction Generator (HIJING) for generating the initial conditions
- Zhang's Parton Cascade (ZPC) for modeling partonic scatterings
- A Relativistic Transport (ART) model for treating hadronic scatterings

AMPT – def treats the initial condition as strings and minijets and using Lund string fragmentation

AMPT – SM treats the initial condition as partons and uses a simple coalescence model to describe hadronization

Perturbative QCD Calculations

Leading Order Calculations (I. Vitev *et al*)

LO single inclusive hadron production cross section

$$\begin{aligned} \frac{d\sigma}{dyd^2p_T} &= K \frac{\alpha_s^2}{s} \sum_{a,b,c} \int \frac{dx_1}{x_1} d^2k_{T_1} f_{a/N}(x_1, k_{T_1}^2) \int \frac{dx_2}{x_2} d^2k_{T_2} f_{b/N}(x_2, k_{T_2}^2) \\ &\times \int \frac{dz_c}{z_c^2} D_{h/c}(z_c) H_{ab \rightarrow c}(\hat{s}, \hat{t}, \hat{u}) \delta(\hat{s} + \hat{t} + \hat{u}) \end{aligned}$$

Gaussian form of k_T dependence in parton densities assumed

$$f_{a/N}(x_1, k_{T_1}^2) = f_{a/N}(x_1) \frac{1}{\pi \langle k_T^2 \rangle} e^{-k_{T_1}^2 / \langle k_T^2 \rangle}$$

In pp collisions, $\langle k_T^2 \rangle_{pp} = 1.8 \text{ GeV}^2/c^2$

Broadening increased in cold matter, $\langle k_T^2 \rangle_{pA} = \langle k_T^2 \rangle_{pp} + \langle 2\mu^2 L / \lambda_{q,g} \rangle \zeta$

Cold matter energy loss due to medium-induced gluon Bremsstrahlung, implemented as a shift in momentum fraction, $f_{i/p}(x) \longrightarrow f_{i/p}(x/(1 - \epsilon_{i,\text{eff}}))$ where $\epsilon \propto \sum_i \Delta E_i / E$ with the sum over all medium-induced gluons

Dynamical shadowing shifts nuclear parton momentum fraction so that

$$f_{i/p}(x) \longrightarrow f_{i/p}((x/ - \hat{t})(1 + C_i \zeta_i^2 (A^{1/3} - 1)))$$

Proton and neutron number (isospin) accounted for

LO/NLO pQCD, w/out Energy Loss (G. Barnafoldi *et al*)

kTpQCD_v2.0 assumes collinear factorization up to NLO

$$E_h \frac{d\sigma_h^{pp}}{d^3p_T} = \frac{1}{s} \sum_{abc} \int_{VW/z_c}^{1-(1-V)/z_c} \frac{dv}{v(1-v)} \int_{VW/vz_c}^1 \frac{dw}{w} \int^1 dz_c$$
$$\times \int d^2\vec{k}_{T_1} \int d^2\vec{k}_{T_2} f_{a/p}(x_1, \vec{k}_{T_1}, \mu_F^2) f_{b/p}(x_2, \vec{k}_{T_2}, \mu_F^2)$$
$$\times \left[\frac{d\tilde{\sigma}}{dv} \delta(1-w) + \frac{\alpha_s(\mu_R)}{\pi} K_{ab,c}(\hat{s}, v, w, \mu_F, \mu_R, \mu_{Fr}) \right] \frac{D_c^h(z_c, \mu_{Fr}^2)}{\pi z_c^2}.$$

$d\tilde{\sigma}/dv$ is LO cross section with next-order correction term $K_{ab,c}(\hat{s}, v, w, \mu_F, \mu_R, \mu_{Fr})$

Proton and parton level NLO kinematic variables are (s, V, W) and (\hat{s}, v, w)

k_T broadening implemented similar to previous LO calculation with

$$\langle k_T^2 \rangle_{pA} = \langle k_T^2 \rangle_{pp} + Ch_{pA}(b)$$

$$h_{pA}(b) = \begin{cases} \nu_A(b) - 1 & \nu_A(b) < \nu_m \\ \nu_m - 1 & \text{otherwise} \end{cases}$$

Shadowing implemented through available parameterizations: EKS98, EPS08, HKN, and HIJING2.0 – scale dependence included

$$f_{a/A}(x, \mu_F^2) = S_{a/A}(x, \mu_F^2) \left[\frac{Z}{A} f_{a/p}(x, \mu_F^2) + \left(1 - \frac{Z}{A}\right) f_{a/n}(x, \mu_F^2) \right]$$

NLO Shadowing Calculation (K. J. Eskola *et al*)

Calculate π^0 production at NLO, compared to charged particle R_{AA}

Only modifications of the parton PDFs in nuclei included

Improved spatial dependence of nPDFs on both EKS98 and EPS09 using power series expansion in the nuclear thickness function

$$r_i^A(x, Q^2, \mathbf{s}) = 1 + \sum_{j=1}^n c_j^i(x, Q^2) [T_A(\mathbf{s})]^j$$

They use the A dependence of the global (min bias) nPDFs to fix coefficients c_j^i

Found $n = 4$ sufficient for reproducing the A systematics

Used INCNLO package with CTEQ6M and KKP, AKK and fDSS fragmentation functions, uncertainties calculated with EPS09(s) error sets and fDSS

The modification factor $R_{p\text{Pb}}$ is calculated as

$$R_{p\text{Pb}}^{\pi^0}(p_T, y; b_1, b_2) \equiv \frac{\left\langle \frac{d^2 N_{p\text{Pb}}^{\pi^0}}{dp_T dy} \right\rangle_{b_1, b_2}}{\frac{\langle N_{\text{coll}}^{p\text{Pb}} \rangle_{b_1, b_2}}{\sigma_{\text{in}}^{NN}} \frac{d^2 \sigma_{\text{pp}}^{\pi^0}}{dp_T dy}} = \frac{\int_{b_1}^{b_2} d^2 \mathbf{b} \frac{d^2 N_{p\text{Pb}}^{\pi^0}(\mathbf{b})}{dp_T dy}}{\int_{b_1}^{b_2} d^2 \mathbf{b} T_{p\text{Pb}}(\mathbf{b}) \frac{d^2 \sigma_{\text{pp}}^{\pi^0}}{dp_T dy}}$$

b_1 and b_2 are centrality-based limits with $b_1 = 0$ and $b_2 \rightarrow \infty$ in min bias collisions

Charged particle and π^0 $R_{p\text{Pb}}$ may be different because of greater baryon contribution in pA collisions, at least in some parts of phase space

Charged Particle Multiplicity and p_T Distributions: Midrapidity

$dN_{\text{ch}}/d\eta$ in Lab Frame

Most calculations done in CM Frame, shift to lab frame involves a shift of $\Delta y_{NN} = 0.465$ in the direction of the proton beam

Test beam data taken with Pb beam moving toward forward rapidity (to the right)

Data do not favor saturation, slope from p side to Pb side is too steep (see next slide)

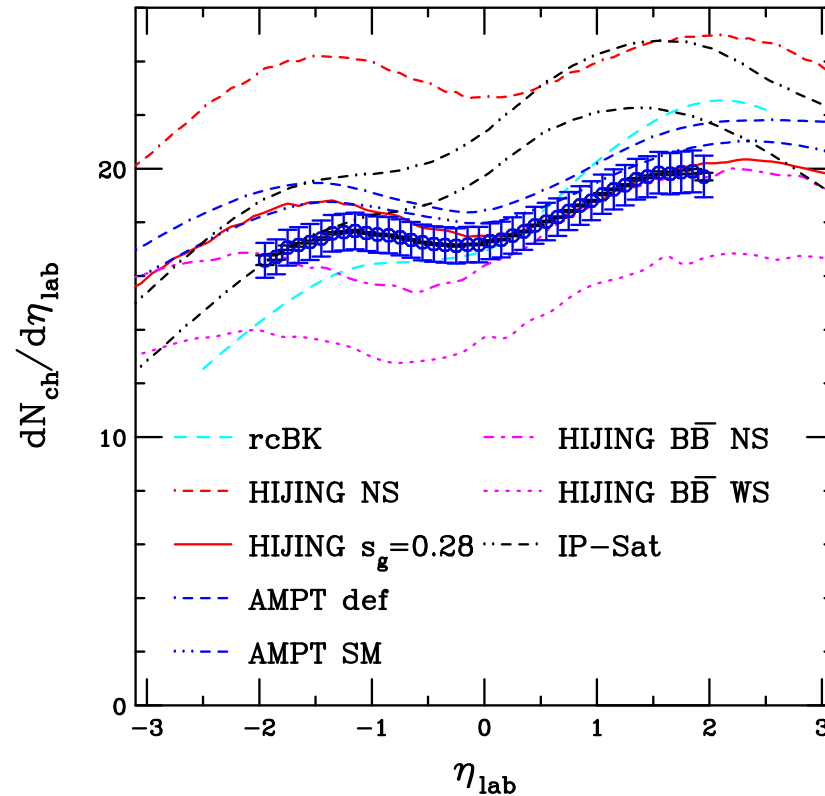


Figure 1: Charged particle pseudorapidity distributions at $\sqrt{s_{NN}} = 5.02$ TeV in the lab frame. Courtesy of Albacete *et al.*, XN Wang *et al.*, Z Lin, Rezaeian, and Topor Pop *et al.* The ALICE data from Phys. Rev. Lett. 110 (2013) 082302 are shown.

CGC Results Depend on Jacobian

The steepness of the slope of $dN_{\text{ch}}/d\eta$ depends on the Jacobian, not calculable in CGC framework but required for $y \rightarrow \eta$ transformation

Calculation by Albacete *et al* assumed same transformation in pp and $p+\text{Pb}$ collisions

New result based on ‘tuned’ Jacobian with modification of hadron momentum by $\Delta P(\eta)$, shows the sensitivity of this result to mean mass and p_T of final-state hadrons

Fixed minijet mass (related to pre-hadronization/fragmentation stage) is assumed – can’t be extracted in CGC, problem largest on the nuclear side

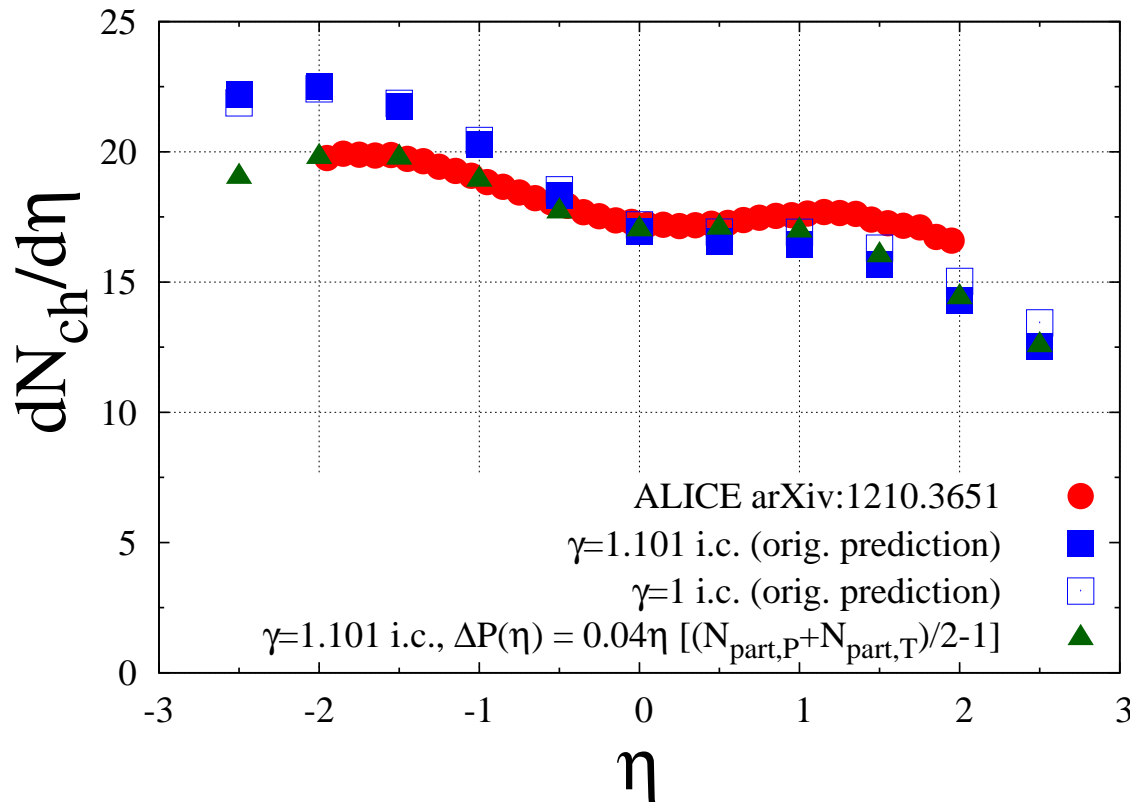


Figure 2: Charged particle pseudorapidity distributions at $\sqrt{s_{NN}} = 5.02$ TeV with and without tuned Jacobian. Courtesy of Albacete *et al.*. Note that here the proton moves to the right (positive y).

Centrality Dependence of $dN_{\text{ch}}/d\eta$

Left-hand side compares AMPT (Z. Lin) with b-CGC (A. Rezaeian)

Right-hand side is preliminary ATLAS data

Results are qualitatively similar

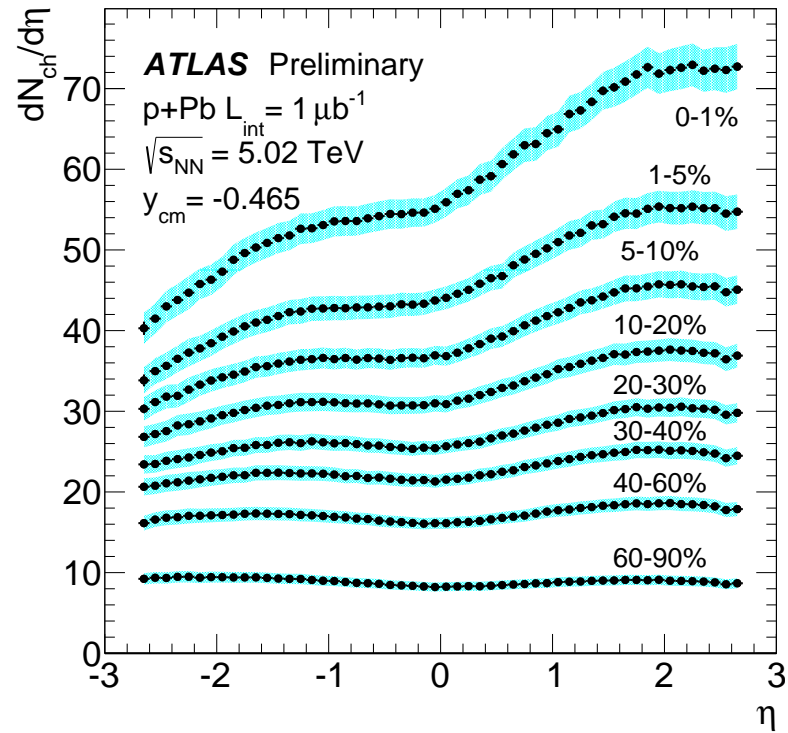
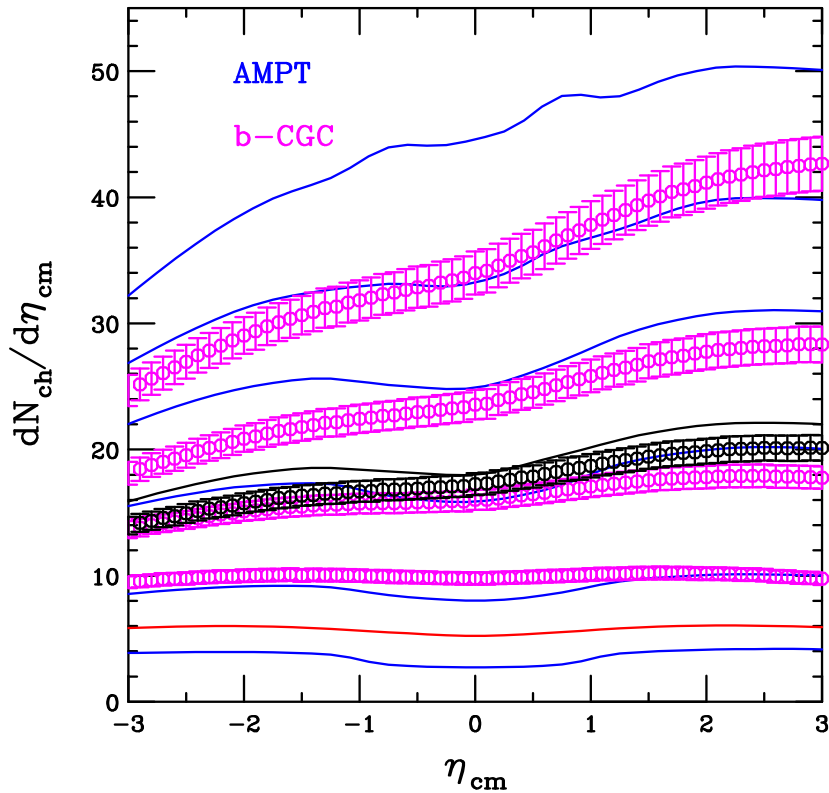


Figure 3: (Left) Charged particle pseudorapidity distributions in the center of mass frame of $p+\text{Pb}$ collisions at various centralities for AMPT (blue, from top to bottom 0-10%, 10-20%, 20-40%, 40-60%, 60-80% and 80-100%; black, min bias; and pp , red) and the b-CGC saturation model (points, from top to bottom, 0-20%, 20-40%, 40-60% and 60-80%; black, min bias). (Right) The ATLAS multiplicity distributions, binned in centrality.

Charged Particle p_T Distributions

Results similar at low p_T but deviate significantly at higher p_T

rcBK distributions do not differ strongly between $\eta = 0$ and 2

HIJING2.0 without shadowing better at low p_T , with better at high p_T

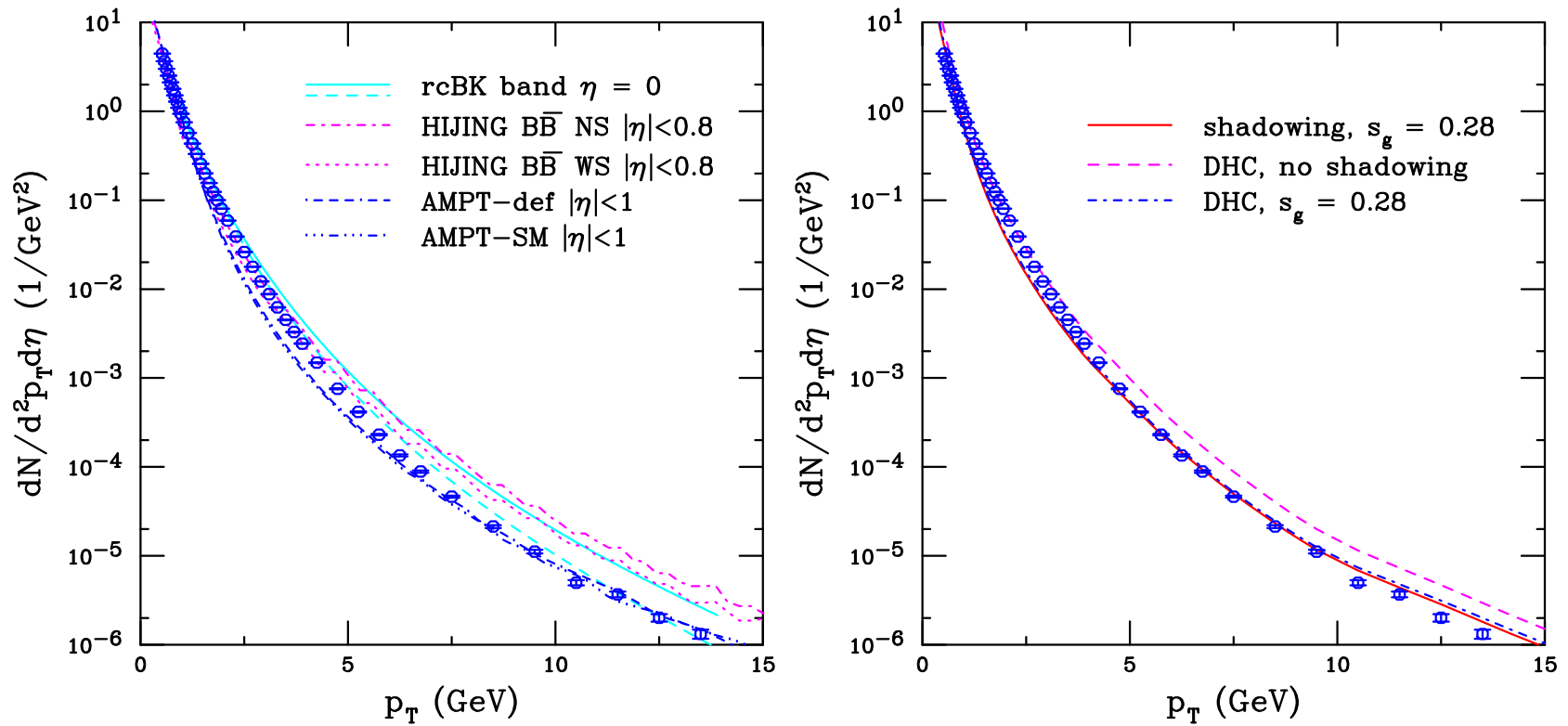


Figure 4: (Left) Charged particle p_T distributions at $\sqrt{s_{NN}} = 5.02$ TeV. The solid and dashed cyan curves outline the rcBK band calculated by Albacete *et al.*. The magenta curves, calculated with HIJINGBB $\bar{\bar{2}}$.0 are presented without (dot-dashed) and with (dotted) shadowing. The AMPT results are given by the dot-dash-dash-dashed (default) and dot-dot-dot-dashed (SM) blue curves. The data are from the ALICE Collaboration, Phys. Rev. Lett. 110 082302 (2013). (Right) The charged hadron p_T distribution in p +Pb collisions with different HIJING2.1 options is also compared to the ALICE data.

R_{pPb} at Midrapidity: Saturation

Large bands for saturation predictions (rcBK, Albacete and Rezaeian; IP-Sat, Tribedy and Venugopalan)

Only the rcBK prediction by Albacete *et al* brackets most of the data

How applicable are CGC calculations above saturation scale?

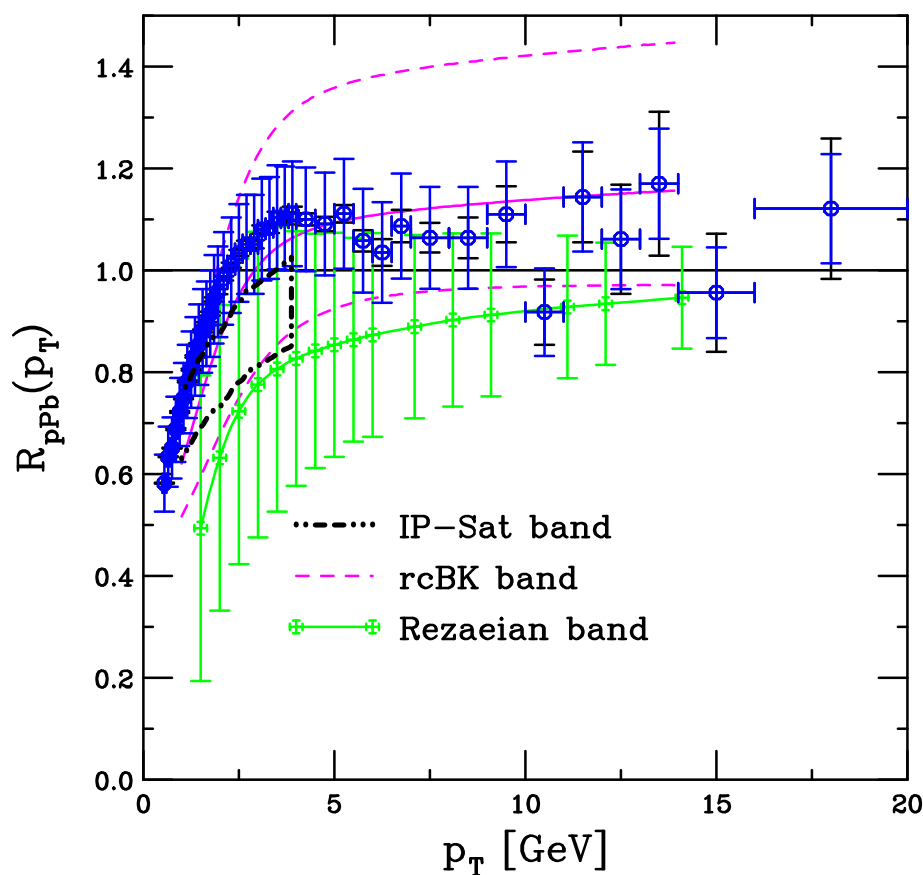


Figure 5: Charged particle $R_{pPb}(p_T)$ at $\sqrt{s_{NN}} = 5.02$ TeV at $\eta \sim 0$. The bands from saturation models by Albacete *et al.* and Rezaeian (rcBK) and Tribedy & Venugopalan (IP-Sat) are compared to the ALICE data (Phys. Rev. Lett. 110 (2013) 082302).

R_{pPb} at Midrapidity: Shadowing I

Standard shadowing parameterizations predict small effect, weak p_T dependence
Calculation by Kopeliovich does best at low p_T

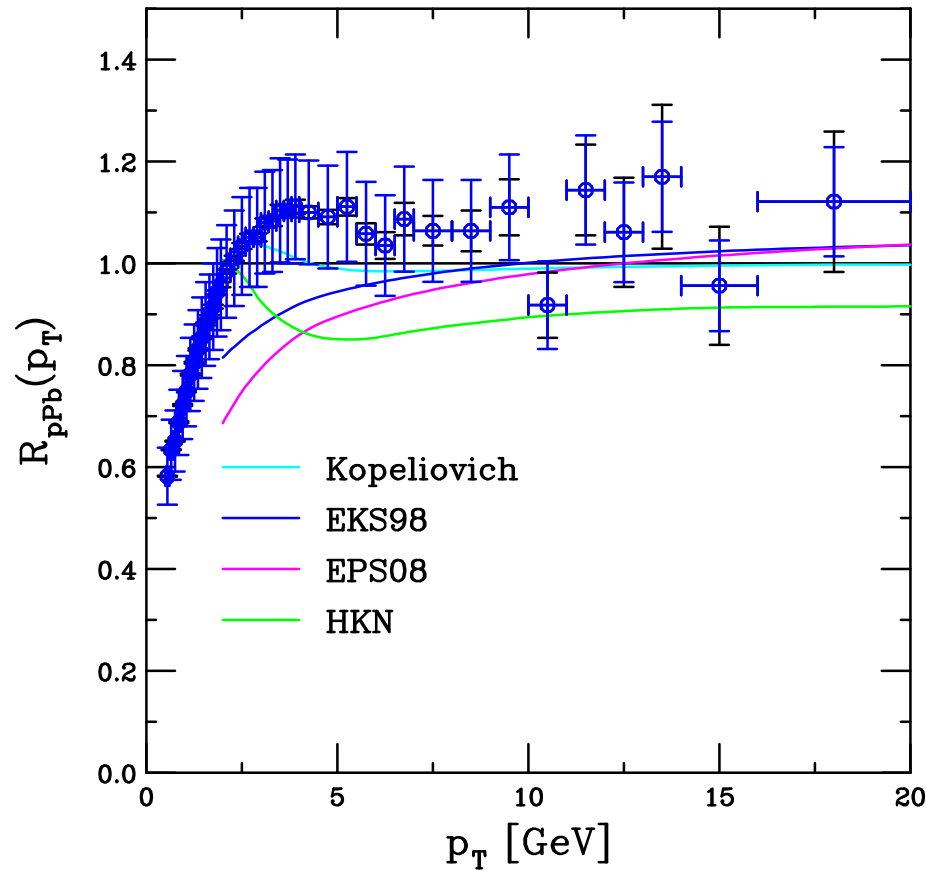


Figure 6: Charged particle $R_{pPb}(p_T)$ at $\sqrt{s_{NN}} = 5.02$ TeV at $\eta \sim 0$. Results with more ‘standard’ shadowing (Barnafoldi *et al.*, Kopeliovich) are compared to the ALICE data (Phys. Rev. Lett. 110 (2013) 082302).

R_{pPb} at Midrapidity: Shadowing II

LO Vitev result includes Cronin effect, cold matter energy loss, and shadowing, difference is whether parameters change with \sqrt{s} or not, agrees at low p_T but falls below at higher p_T

EPS09 min bias band for π^0 also shown, only nPDF effects taken into account, not inconsistent with data

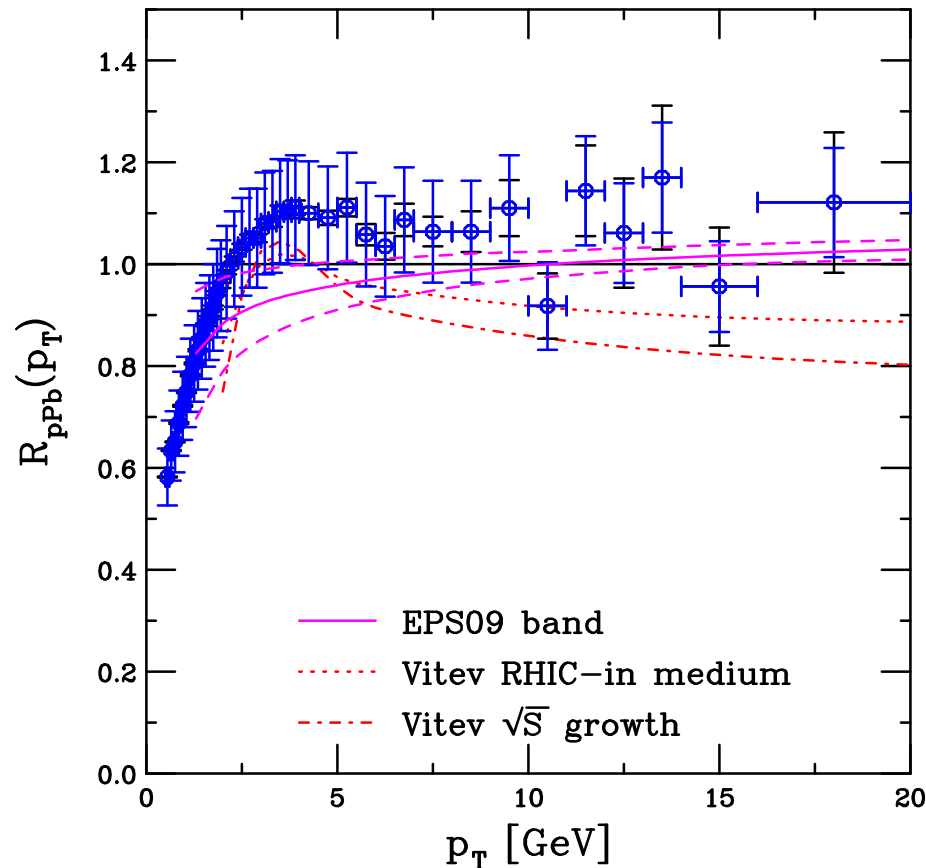


Figure 7: Charged particle $R_{pPb}(p_T)$ at $\sqrt{s_{NN}} = 5.02$ TeV at $\eta \sim 0$. The cold matter calculations by Vitev and collaborators include energy loss while those by Eskola and collaborators does not. The ALICE data (Phys. Rev. Lett. 110 (2013) 082302) are also shown.

R_{pPb} at Midrapidity: Shadowing III

EPS09 min bias band for π^0 also shown, only nPDF effects taken into account
 π^0 result does not include baryons which could be present in charged particle ratios
CMS

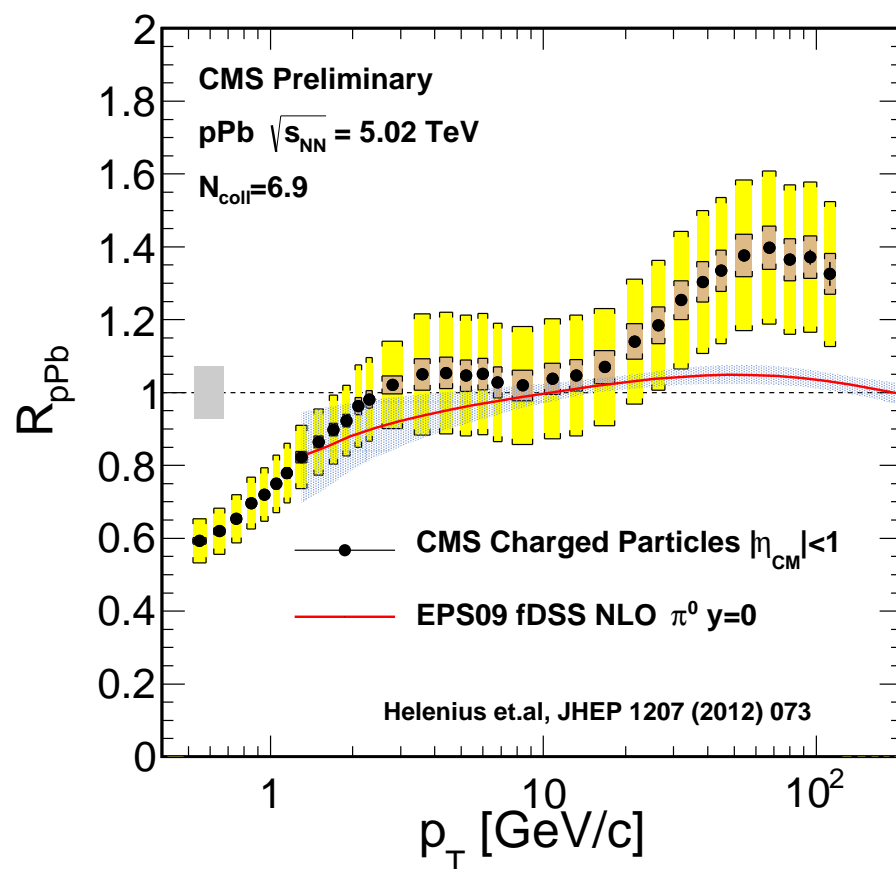


Figure 8: Charged particle $R_{pPb}(p_T)$ at $\sqrt{s_{NN}} = 5.02$ TeV at $|\eta| \leq 1$ measured by CMS (HP13). The calculation is the π^0 result by Eskola *et al.*

$R_{p\text{Pb}}$ at Midrapidity: Generators

HIJINGBB $\bar{\bar{}}$ shows large differences in $R_{p\text{Pb}}$ due to shadowing but AMPT modes do not differ much

HIJING2.0 should improve at higher p_T if scale evolution of nPDFs included

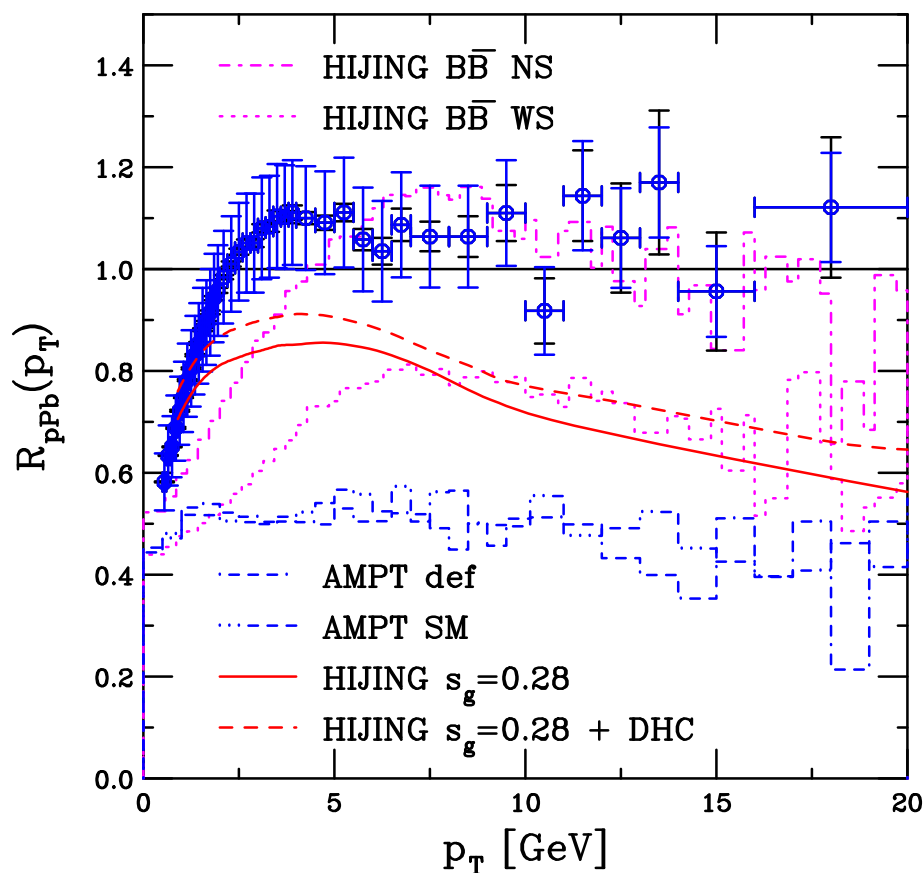


Figure 9: Charged particle $R_{p\text{Pb}}(p_T)$ at $\sqrt{s_{NN}} = 5.02$ TeV at $\eta \sim 0$. HIJINGBB $\bar{\bar{}}$ (Topor Pop *et al.*) with and without shadowing compared to AMPT (Z. Lin) default and with string melting. The difference in the HIJING curves depends on whether the hard scatterings are coherent or not. The ALICE data (Phys. Rev. Lett. 110 (2013) 082302) are also shown.

J/ψ

Pinning Down Open Charm Uncertainties by Fitting $\sigma_{c\bar{c}}$

Caveat: full NNLO cross section unknown, could still be large corrections

Employ $m = 1.27$ GeV, lattice value at $m(3\text{ GeV})$ and use subset of $c\bar{c}$ total cross section data to fix best fit values of μ_F/m and μ_R/m

Result with $\Delta\chi^2 = 1$ gives uncertainty on scale parameters; $\Delta\chi^2 = 2.3$ gives one standard deviation on total cross section

LHC results from ALICE agrees well even though not included in the fits

Same mass and scale parameters used to calculate J/ψ

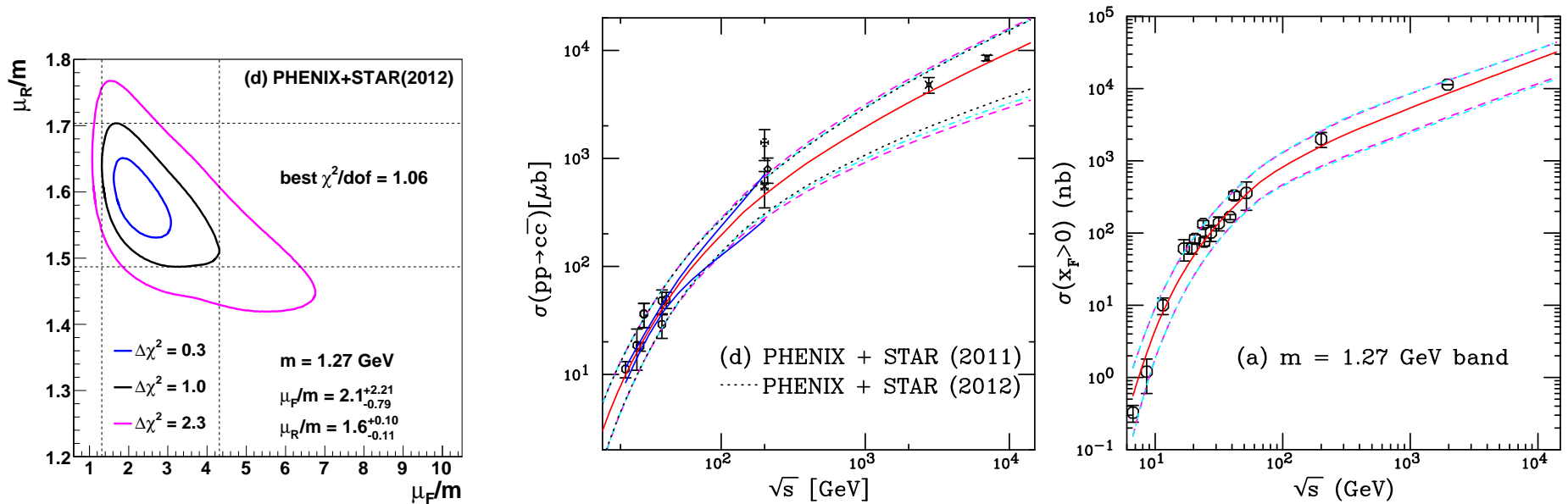


Figure 10: (Left) The χ^2/dof contours for fits including the STAR 2011 cross section but excluding the STAR 2004 cross section. The best fit values are given for the furthest extent of the $\Delta\chi^2 = 1$ contours. (Center) The energy dependence of the charm total cross section compared to data. The best fit values are given for the furthest extent of the $\Delta\chi^2 = 1$ contours. The central value of the fit in each case is given by the solid red curve while the dashed magenta curves and dot-dashed cyan curves show the extent of the corresponding uncertainty bands. The dashed curves outline the most extreme limits of the band. In addition, the dotted black curves show the uncertainty bands obtained with the 2012 STAR results while the solid blue curves in the range $19.4 \leq \sqrt{s} \leq 200$ GeV represent the uncertainty obtained from the extent of the $\Delta\chi^2 = 2.3$ contour. (Right) The uncertainty band on the forward J/ψ cross section. The dashed magenta curves

Calculating Uncertainties in pA

The one standard deviation uncertainties on the quark mass and scale parameters calculated using EPS09 central set

If the central, upper and lower limits of $\mu_{R,F}/m$ are denoted as C , H , and L respectively, then the seven sets corresponding to the scale uncertainty are

$$(\mu_F/m, \mu_F/m) = (C, C), (H, H), (L, L), (C, L), (L, C), (C, H), (H, C)$$

The extremes of the cross sections with mass and scale are used to calculate the uncertainty

$$\begin{aligned}\sigma_{\max} &= \sigma_{\text{cent}} + \sqrt{(\sigma_{\mu, \max} - \sigma_{\text{cent}})^2 + (\sigma_{m, \max} - \sigma_{\text{cent}})^2}, \\ \sigma_{\min} &= \sigma_{\text{cent}} - \sqrt{(\sigma_{\mu, \min} - \sigma_{\text{cent}})^2 + (\sigma_{m, \min} - \sigma_{\text{cent}})^2},\end{aligned}$$

Uncertainties due to shadowing calculated using 30+1 error sets of EPS09 NLO added in quadrature, uncertainty is cumulative

Final-State Energy Loss (Arleo and Peigne)

Arleo and Peigne fit an energy loss parameter that also depends on L_A to E866 data and uses the same parameter for other energies

$$\frac{1}{A} \frac{d\sigma_{pA}(x_F)}{dx_F} = \int_0^{E_p - E} d\epsilon P(\epsilon) \frac{d\sigma_{pp}(x_F + \delta x_F(\epsilon))}{dx_F}$$

There is no production model, only a parameterization of the pp cross section

$$\frac{d\sigma_{pp}}{dp_T dx} = \frac{(1-x)^m}{x} \left(\frac{p_0^2}{(p_0^2 + p_T^2)} \right)^m$$

Parameters n and m are fit to pp data, $n \sim 5$ at $\sqrt{s} = 38.8$ GeV, **34** at **2.76** TeV

Including shadowing as well as energy loss modifies the energy loss parameter, no significant difference in shape of fit at fixed-target energy but significant difference at higher \sqrt{s}

Backward x_F/y effect is large for this scenario

$$R_{pPb}$$

As expected, NLO shadowing alone does not describe curvature of data
 Energy loss with shadowing overestimates effect at forward rapidity
 CGC calculations (not shown) fall even further below data
 R_{pPb} problematic because no measured pp denominator

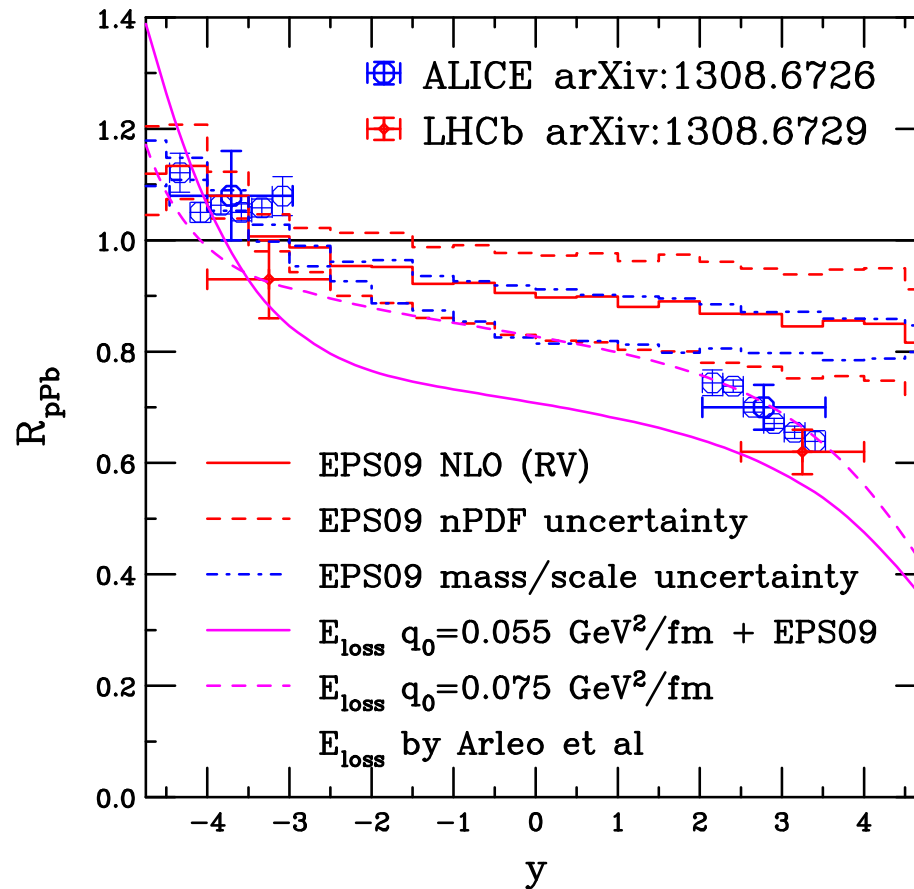


Figure 11: The R_{pPb} ratio for J/ψ as a function of y . The dashed red histogram shows the EPS09 uncertainties while the dot-dashed blue histogram shows the dependence on mass and scale. The pp denominator is also calculated at 5 TeV (which isn't available experimentally). The energy loss calculations of Arleo and Peigne are shown in magenta.

$$R_{F/B}$$

Forward (+ y) to backward ($-y$) ratio preferable because no pp normalization required for data

Data are flatter in y than the calculations

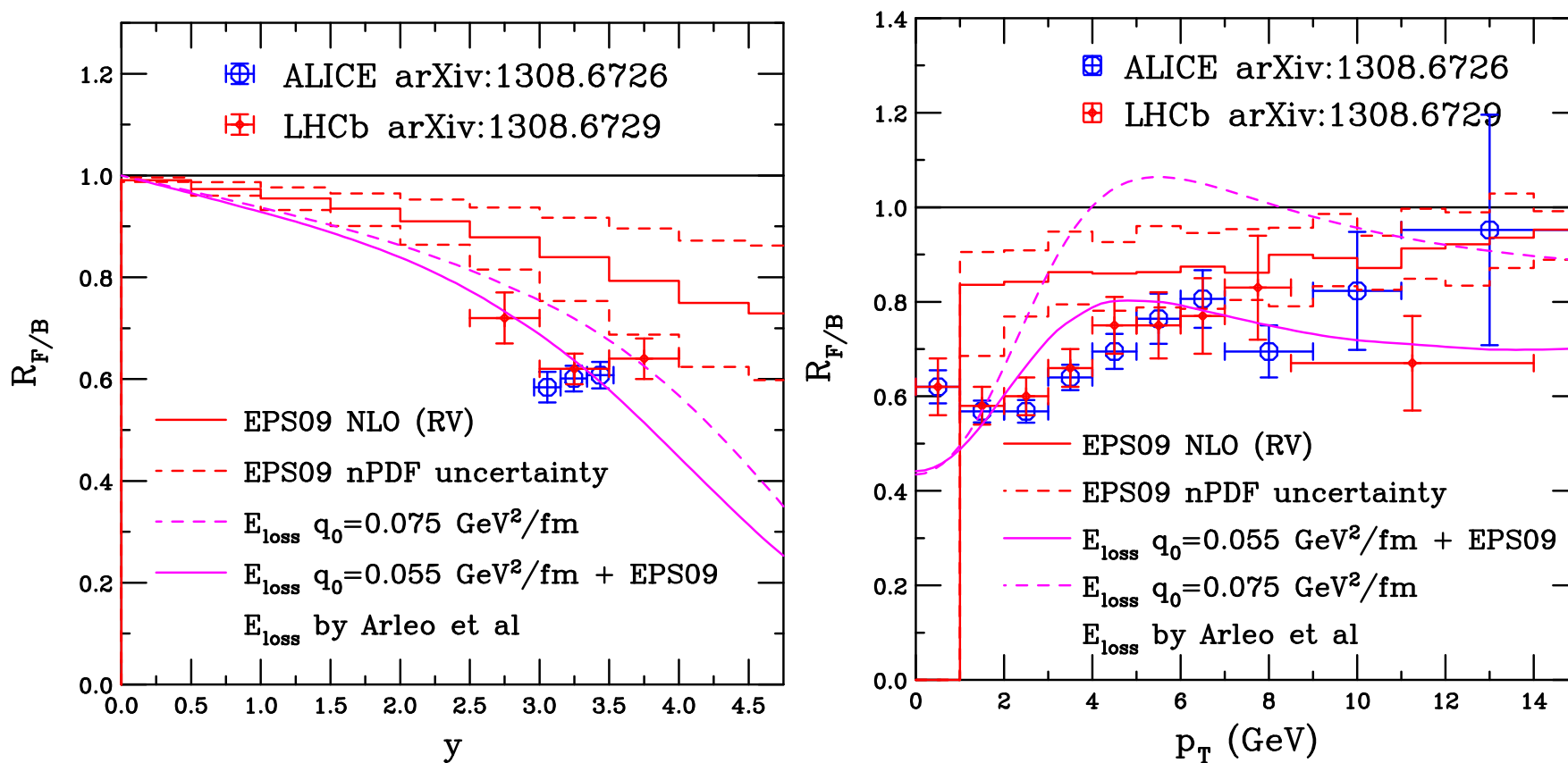


Figure 12: The $R_{F/B}$ ratios for J/ψ as a function of y (left) and p_T (right). The dashed red histogram shows the EPS09 uncertainties. The energy loss calculations of Arleo and Peigne are shown in magenta.

Summary

- p +Pb run at LHC provides interesting studies of cold matter effects in a new energy regime
- The charged particle results for $R_{p\text{Pb}}$ are mostly compatible with pQCD and CGC results, $dN_{\text{ch}}/d\eta$ more difficult to reproduce
- The J/ψ results are compatible with both NLO shadowing and shadowing+energy loss
- Thanks again to everyone who provided predictions and data and plots (Roberta Araldi, Fanfan Jing, Brian Cole, Peter Steinberg, Julia Velkovska, Christoph Roland, and Krisztian Krajczar)
- Watch for updates as more data become available

Relative p and Pb Peak Ratios in Lab Frame

Models without saturation come closer to data as well as getting the forward/backward ratio right

	$dN_{\text{ch}}/d\eta_{\text{lab}}$			$R(\eta_{\text{lab}} = 2/\eta_{\text{lab}} = -2)$
	-2	0	2	
ALICE	16.65 ± 0.65	17.24 ± 0.66	19.81 ± 0.78	1.19 ± 0.05
Saturation Models				
IP-Sat	17.55	20.55	23.11	1.32
KLN	15.96	17.51	22.02	1.38
rcBK	14.27	16.94	22.51	1.58
HIJING-based				
2.1 NS (no shad)	23.58	22.67	24.96	1.06
2.1 WS ($s_g = 0.28$)	18.30	17.49	20.21	1.10
$\overline{\text{B}}\overline{\text{B}}$ NS*	20.03	19.68	23.24	1.16
$\overline{\text{B}}\overline{\text{B}}$ NS [†]	16.84	16.39	19.68	1.16
$\overline{\text{B}}\overline{\text{B}}$ WS*	12.97	12.09	15.16	1.17
$\overline{\text{B}}\overline{\text{B}}$ WS [†]	13.98	13.71	16.73	1.20
AMPT				
Default	19.07	18.56	21.65	1.14
String Melting	18.14	18.10	20.84	1.15
DPMJET	17.50	17.61	20.67	1.18

Table 1: Comparison of values of $dN_{\text{ch}}/d\eta_{\text{lab}}$ at $\eta_{\text{lab}} = -2, 0, 2$ and the ratio $dN_{\text{ch}}/d\eta_{\text{lab}}|_{\eta_{\text{lab}}=2}/dN_{\text{ch}}/d\eta_{\text{lab}}|_{\eta_{\text{lab}}=-2}$, denoted by R above. The * on HIJING $\overline{\text{B}}\overline{\text{B}}$ indicates that the calculations have been shifted to the lab frame by the ALICE Collaboration while the [†] are results provided by V. Topor Pop. Adapted from ALICE Collaboration, arXiv:1210.3615 [nucl-ex].

Charged Particle Multiplicity and p_T Distributions:
 $\eta \neq 0$

$R_{p\text{Pb}}$ at Midrapidity: parton vs. hadrons in HIJING

Large to small Cronin enhancement seen for parton $R_{p\text{Pb}}$

Hadronization reduces enhancement, decoherent scattering mitigates strong shadowing at high p_T , arrow on right-hand plot indicates the direction that HIJING prediction should go if scale evolution of shadowing is included

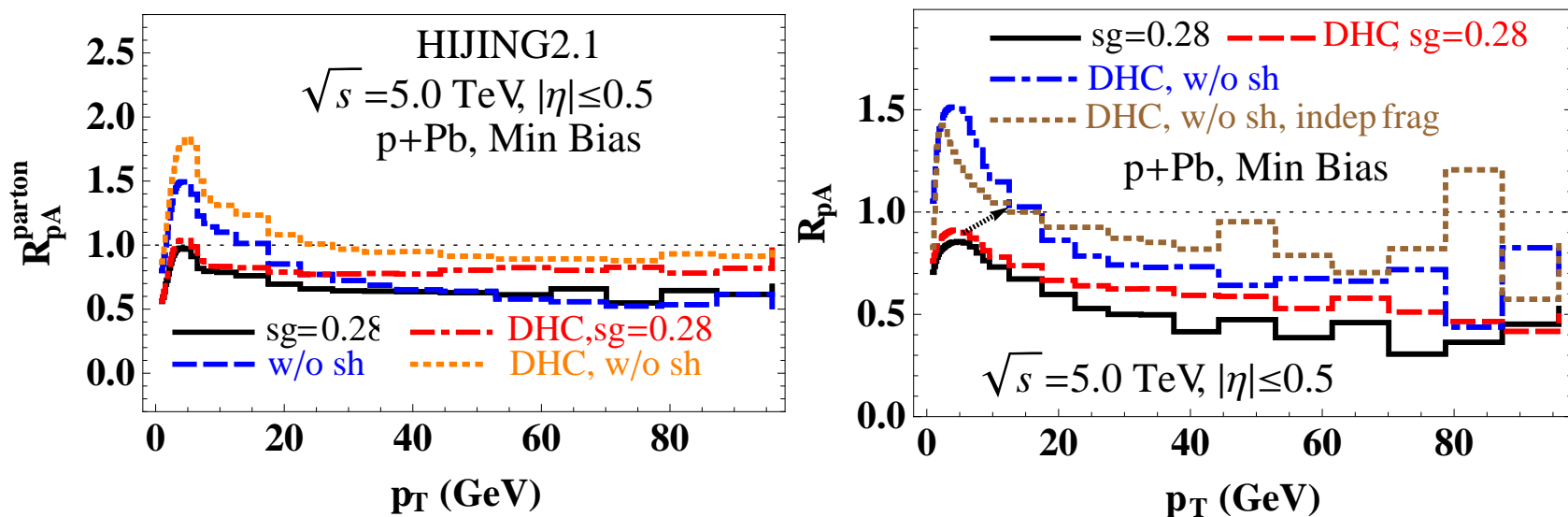


Figure 13: (Left) The nuclear modification factor of the parton p_T spectra in p+Pb collisions. (Right) The charged hadron nuclear modification factor with different HIJING2.1 options. The arrow indicates the most probable trend of the nuclear modification factor to transition from the low to the high p_T regions.

Rezaeian rcBK Rapidity Dependence

Results are shown for different N and α_s^{in} , along with band for scale uncertainty – fixing N from data at one rapidity will fix it for other rapidities as well

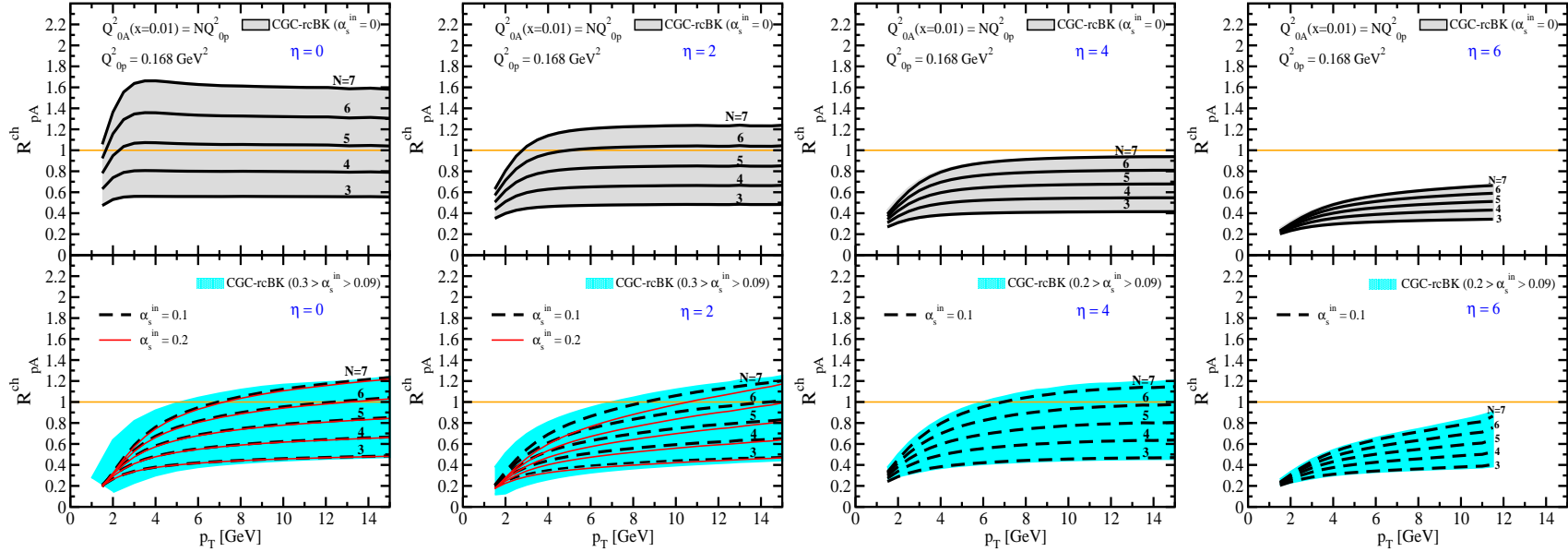


Figure 14: The nuclear modification factor R_{pA}^{ch} for charged hadron production in minimum bias $p+\text{Pb}$ collisions at $\eta = 0, 2, 4,$ and 6 (with the convention that the proton beam moves toward forward rapidity) obtained from hybrid factorization assuming different values of the saturation scale in the nucleus, Q_{0A}^2 . The lines labeled by a given value of N , for $3 < N < 7$, are results with fixed factorization scale $\mu_F = p_T$ and fixed saturation scale $Q_{0A}^2 = N Q_{0p}^2$ and $Q_{0p}^2 = 0.168 \text{ GeV}^2/c^2$. The bands shown the variation in the results with the choice of factorization scale. Two panels are shown for each rapidity. The upper panel shows results obtained by taking $\alpha_s^{\text{in}} = 0$ (assuming only elastic contribution) while the bottom panel shows the variation of α_s^{in} in the range $0.09 \geq \alpha_s^{\text{in}} \geq 0.3$. In the bottom panels for $\eta = 0$ and 2 , results with both $\alpha_s^{\text{in}} = 0.1$ and 0.2 are shown, while for $\eta = 4$ and 6 , only $\alpha_s^{\text{in}} = 0.1$ is shown. The plots are courtesy of Amir Rezaeian.

Albacete *et al* rcBK

Comparison between min bias and two different centralities in $p+\text{Pb}$ collisions are shown for $\eta = 0$ and 2

Uncertainty is largest for min bias, weakest effect (and smallest uncertainty) is for peripheral collisions, $N_{\text{part}} < 5$

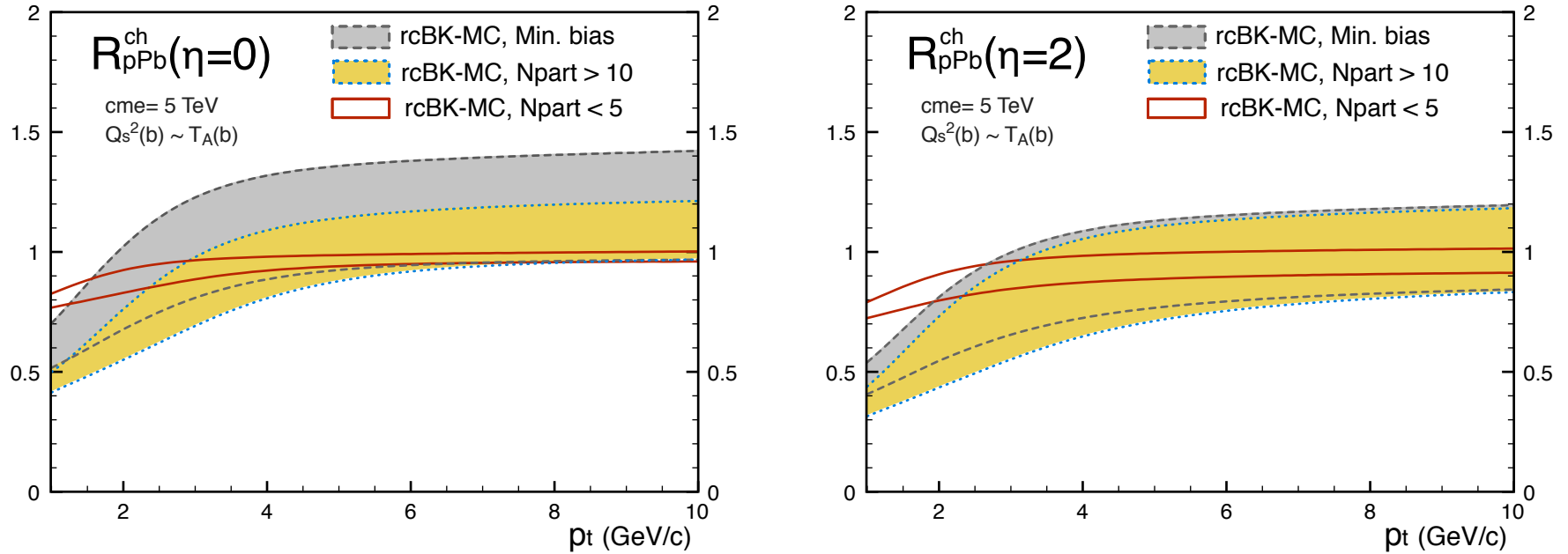


Figure 15: The nuclear modification factor for three different centrality classes assuming k_T -factorization. The $\eta = 2$ result is obtained with the convention that the proton beam moves toward forward rapidity.

Vitev et al Cold Matter Effects

Range of band results from taking the same scattering parameters as at RHIC (upper edge) as well as assuming some enhancement due to the higher energy of the LHC (lower edge)

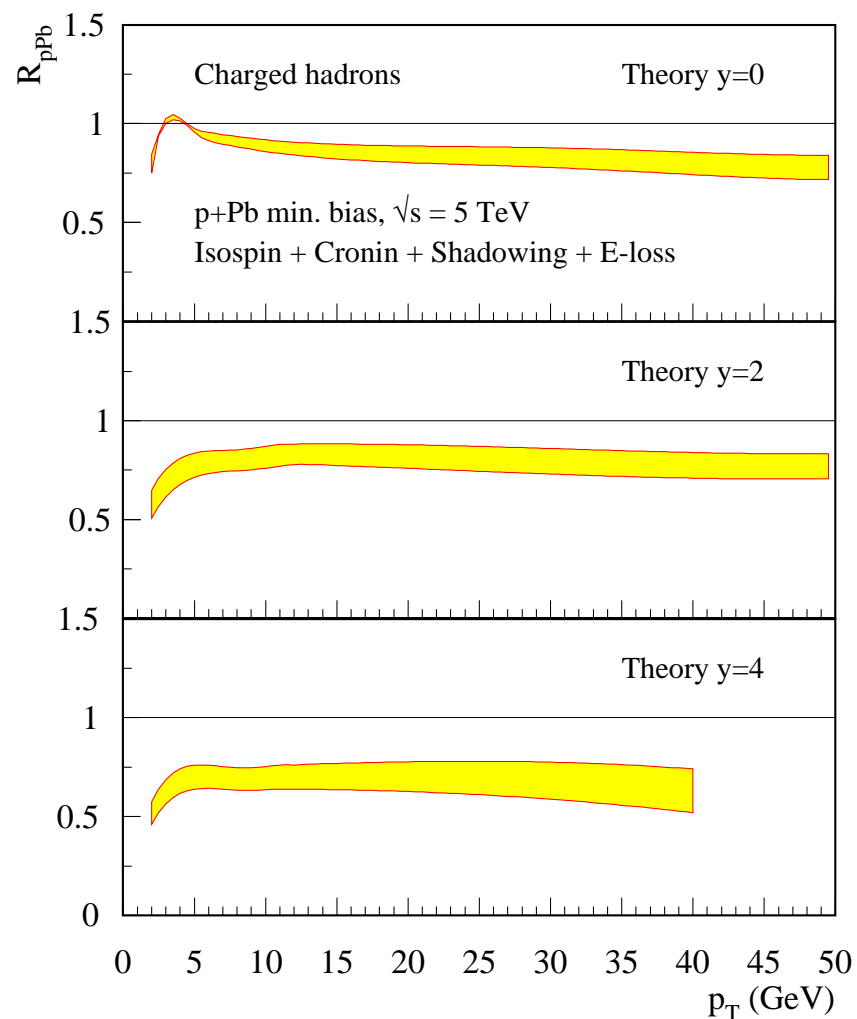


Figure 16: Predictions for the nuclear modification factor R_{pPb} as a function of p_T for charged hadron production in minimum bias p +Pb collisions. Results are shown for three rapidities: $y = 0$ (top), $y = 2$ (center), and $y = 4$ (bottom) with the convention that the proton beam moves toward forward rapidity.

Forward-Backward Asymmetry

$$Y_{\text{asym}}^h(p_T) = \frac{E_h d^3 \sigma_{p\text{Pb}}^h / d^2 p_T d\eta |_{\eta > 0}}{E_h d^3 \sigma_{p\text{Pb}}^h / d^2 p_T d\eta |_{\eta < 0}} = \frac{R_{p\text{Pb}}^h(p_T, \eta > 0)}{R_{p\text{Pb}}^h(p_T, \eta < 0)}$$

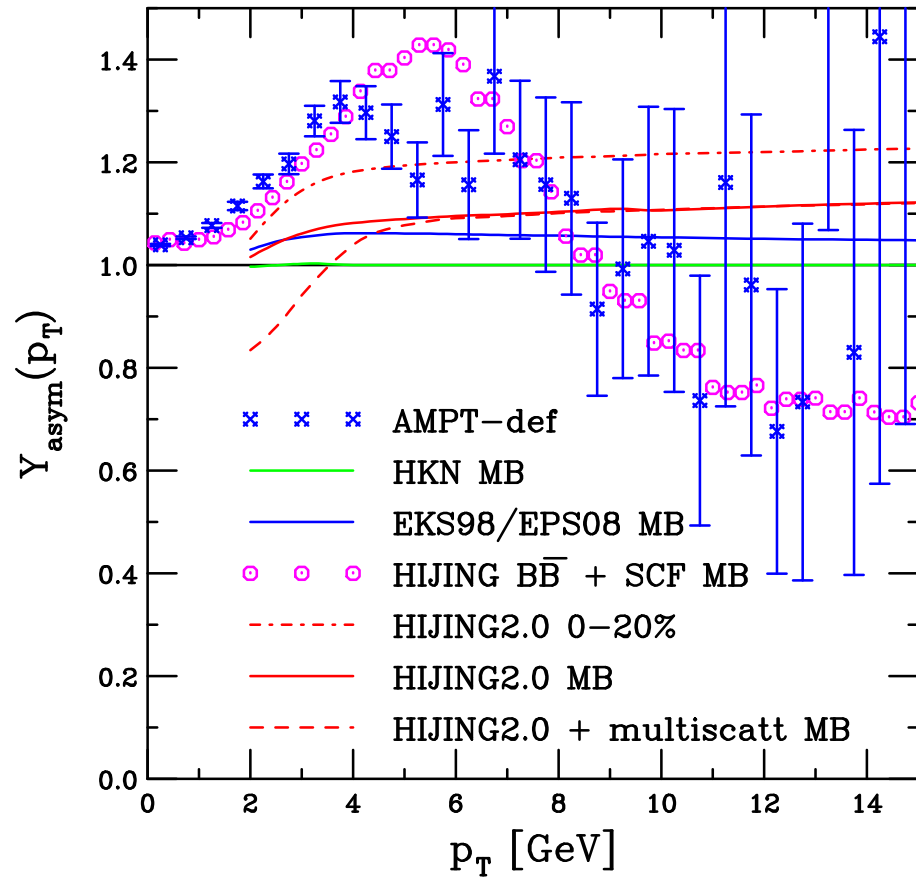


Figure 17: Predictions for the forward-backward asymmetry, $Y_{\text{asym}}^h(p_T)$. Centrality independent results are shown for the HKN, EKS98 and EPS08 parameterizations (labeled MB). Minimum bias results are also shown for HIJING $\text{B}\bar{\text{B}}$ 2.0 and HIJING2.0 with multiple scattering. In addition, HIJING2.0 results in MB collisions and for the 20% most central collisions are also shown. The blue points are the AMPT – def results. Courtesy of G. Barnafoldi *et al.*

Identified Particles

$R_{p\text{Pb}}$ for Neutral Pions

EPS09 shadowing + isospin gives enhancement at $y = 0$, including Cronin and energy loss results in reduction

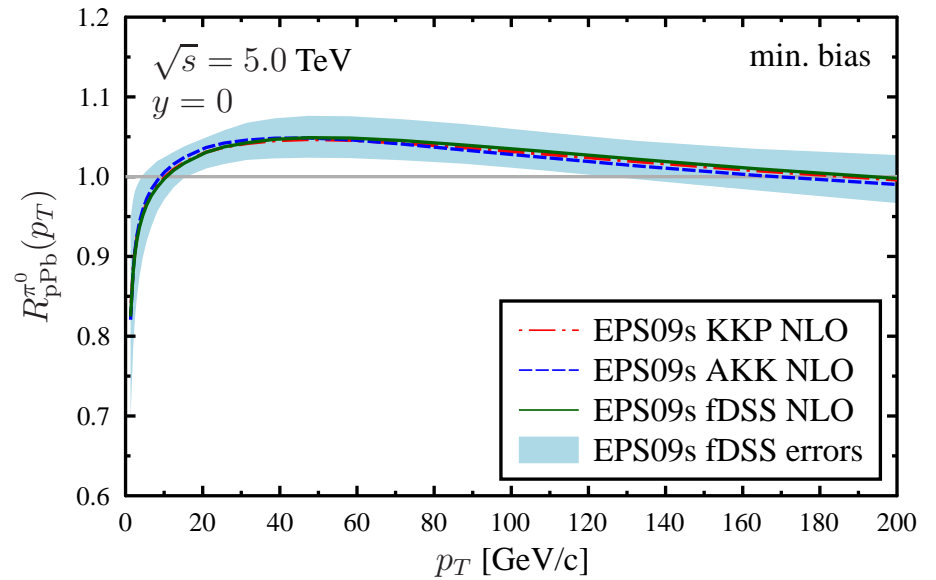
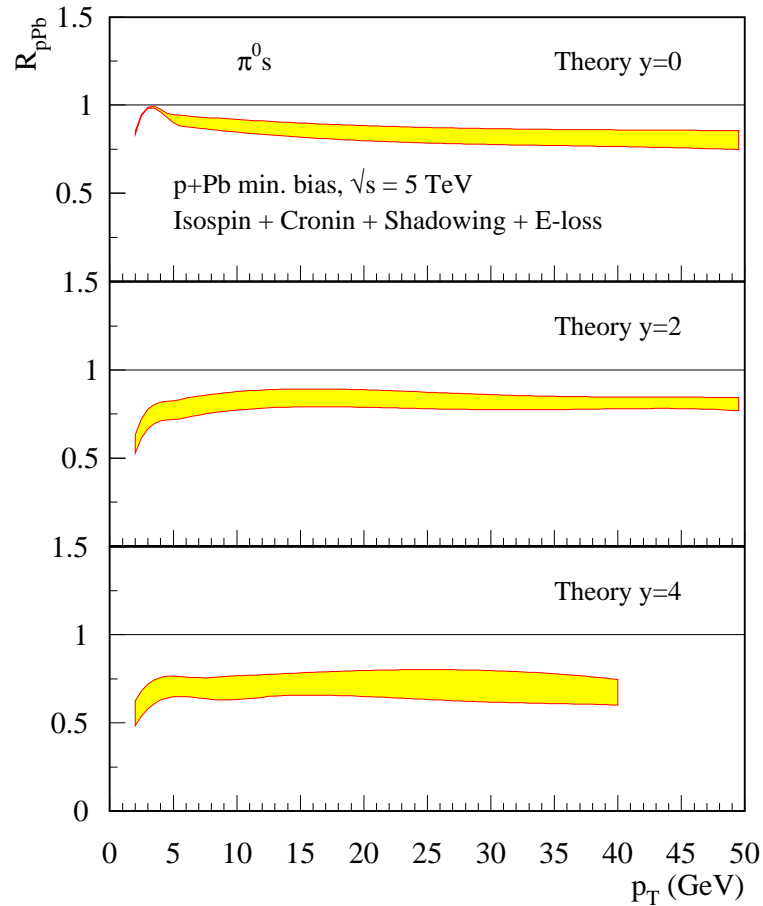


Figure 18: (Left) Vitev *et al.* predictions at $y = 0, 2$ and 4 . (Right) Eskola *et al.* comparing different fragmentation functions as well as delineating the EPS09s uncertainties.

AMPT K^\pm , p , \bar{p} Rapidity Distributions

Definite differences between protons and antiprotons, especially in the direction of motion of the lead nucleus, K^+ and K^- more similar

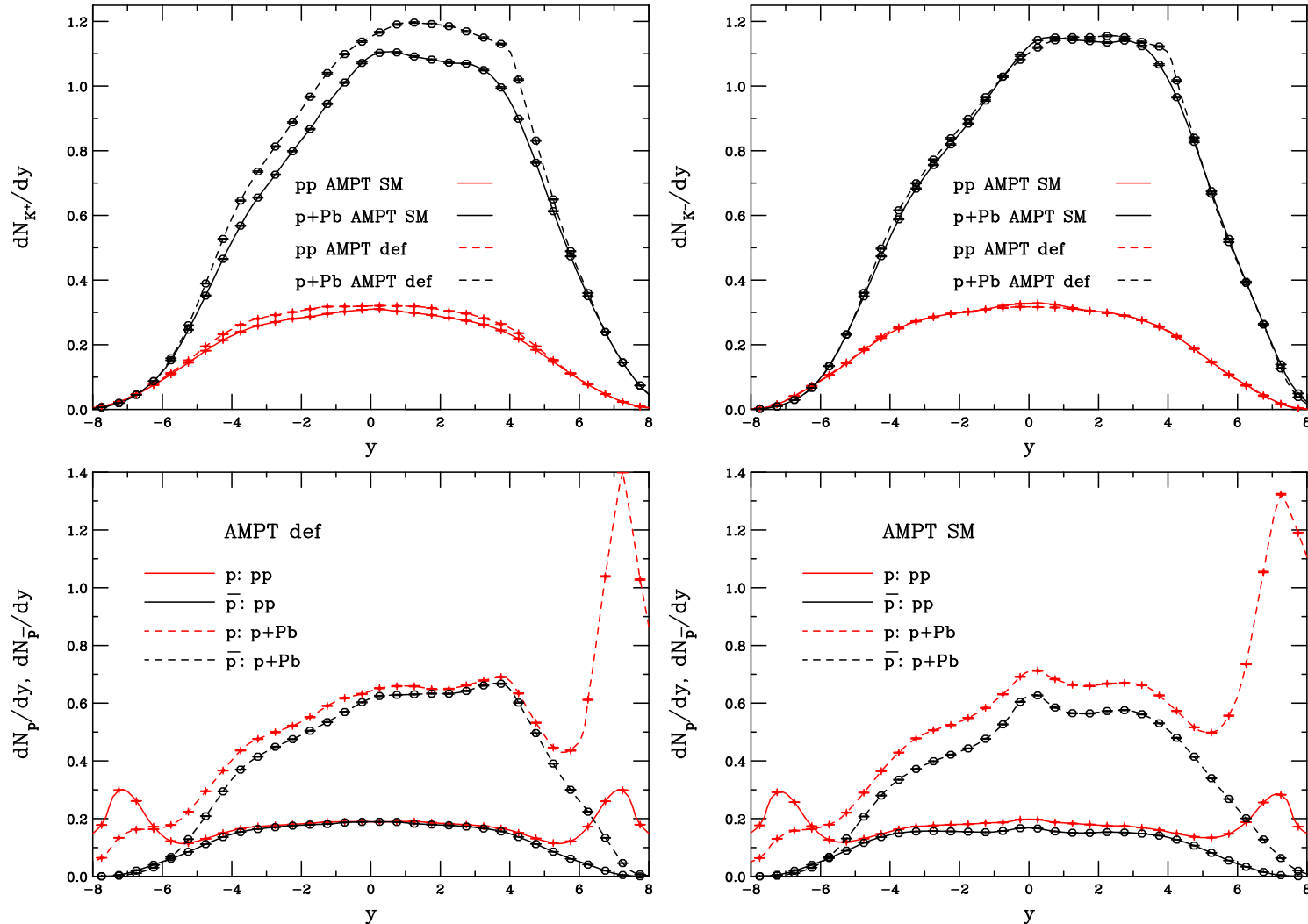


Figure 19: Rapidity distribution, dN/dy , of K^+ (top left) and K^- (top right) mesons and p (bottom left) and \bar{p} (bottom right) baryons.

Jets

Multiple Jet Production in Different Rapidity Intervals

NLO jet cross sections and yields for one, two and three jets

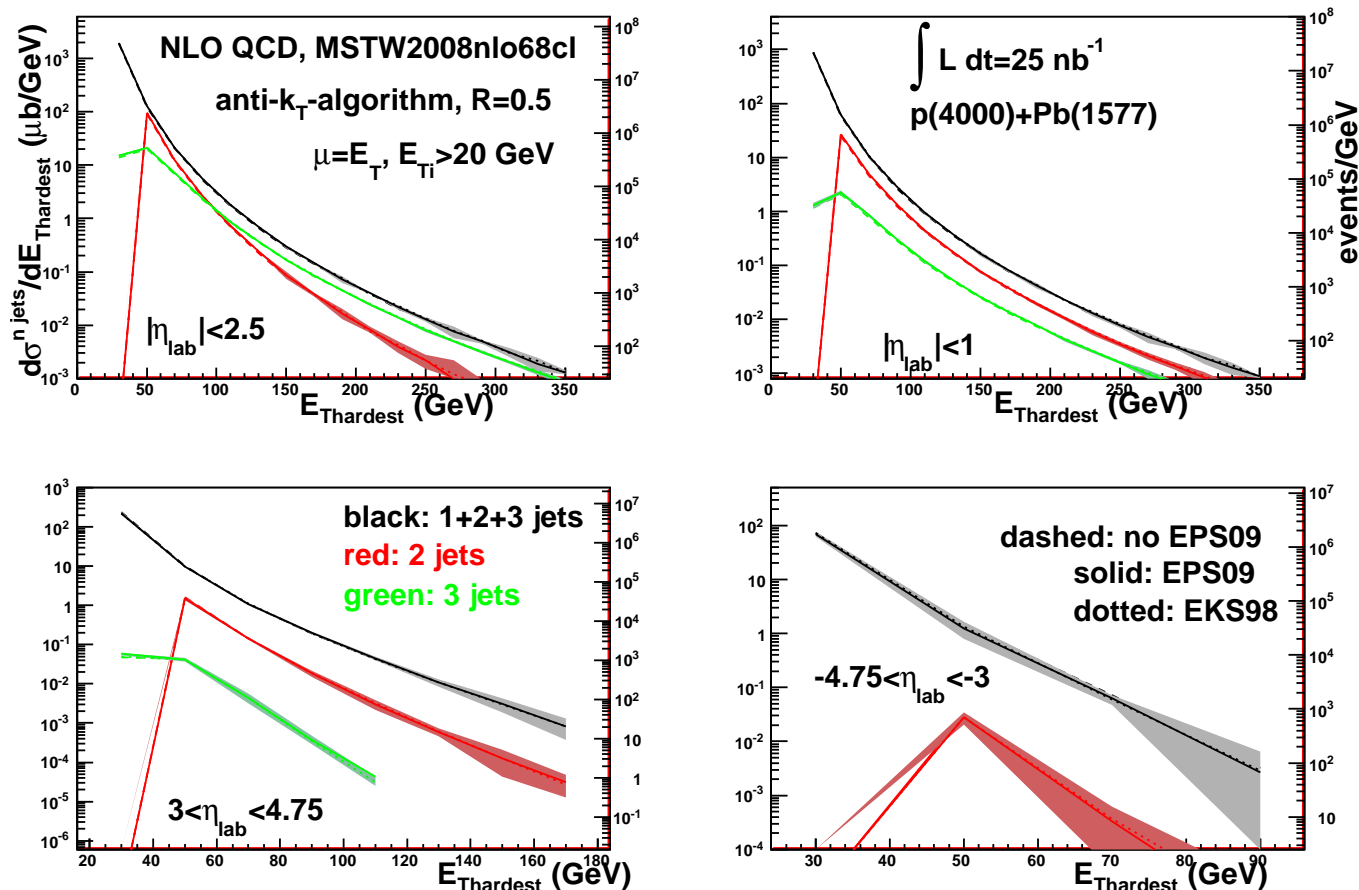


Figure 20: Sum of the one, two and three jets (black), two jets (red) and three jets (green) cross sections as a function of the E_T of the hardest jet within the acceptance. Different pseudorapidity windows (in the lab frame) computed for minimum bias p +Pb collisions at the LHC (4+1.58 TeV per nucleon) are considered. Dashed lines are the results without nuclear modification to the PDFs; solid lines are the results with EPS09NLO; dotted lines are results with EKS98. The bands correspond to the EPS09 uncertainties. The right-hand y -axes give the corresponding yields for an integrated luminosity of 25 nb^{-1} . Courtesy of Nestor Armesto.

Cold Matter Effects on Single and Dijet Production

Cold matter jet R_{pPb} small (NLO calculation at midrapidity, jet cone $R = 0.4$, not a strong function of E_T)

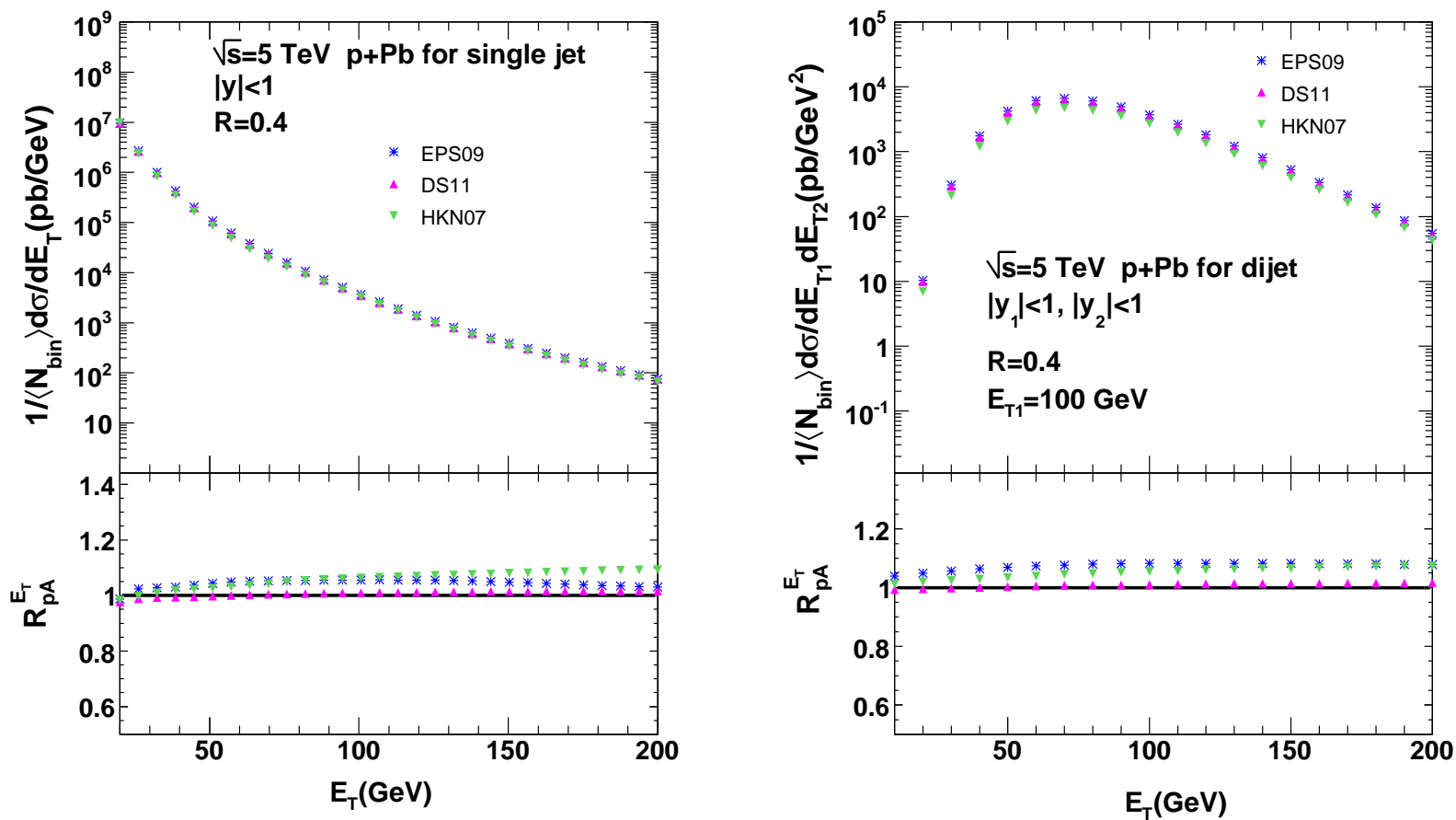


Figure 21: The inclusive jet spectra (left) and dijet E_T spectra with fixed energy $E_{T1} = 100$ GeV (right) in $p+Pb$ collisions at $\sqrt{s} = 5$ TeV and the nuclear modification factors with three sets of nPDFs. Courtesy of Zhang *et al.*.

Azimuthal Decorrelation of Dijets

Dijet cross section for $x_1 \simeq 1$ (DGLAP density), $x_2 \ll 1$ (unintegrated gluon density)

$$\frac{d\sigma}{dy_1 dy_2 dp_{T1} dp_{T2} d\Delta\phi} = \sum_{a,c,d} \frac{p_{T1} p_{T2}}{8\pi^2 (x_1 x_2 s)^2} \mathcal{M}_{ag \rightarrow cd} x_1 f_{a/A}(x_1, \mu^2) \phi_{g/B}(x_2, k_T^2) \frac{1}{1 + \delta_{cd}}$$

$k_T^2 = p_{T1}^2 + p_{T2}^2 + 2p_{T1}p_{T2} \cos \Delta\phi$, $\Delta\phi$ is azimuthal distance between jets

Jet suppression (decorrelation) at $\Delta\phi \sim \pi$ due to saturation effects at large A

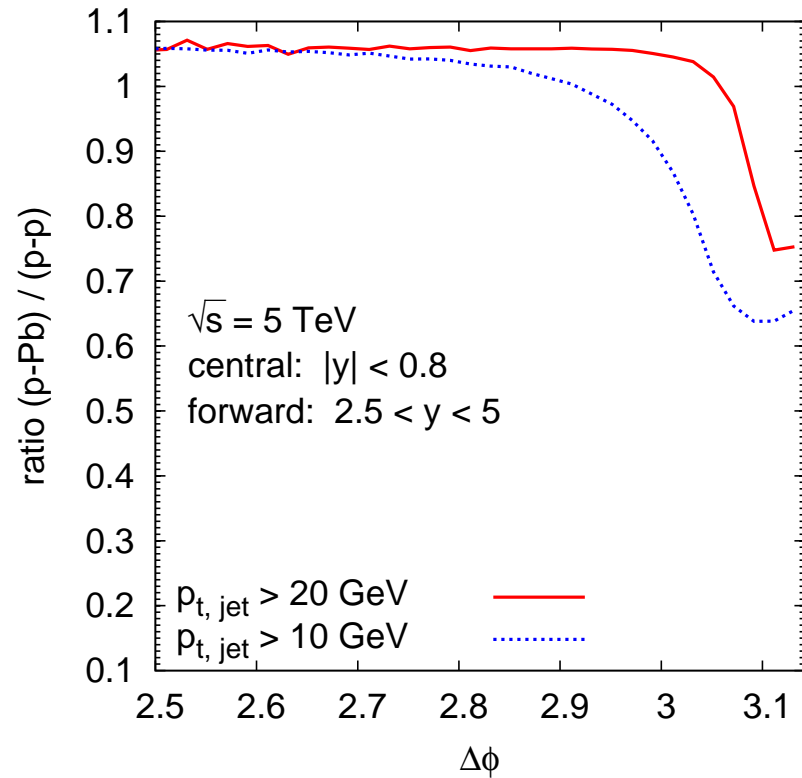
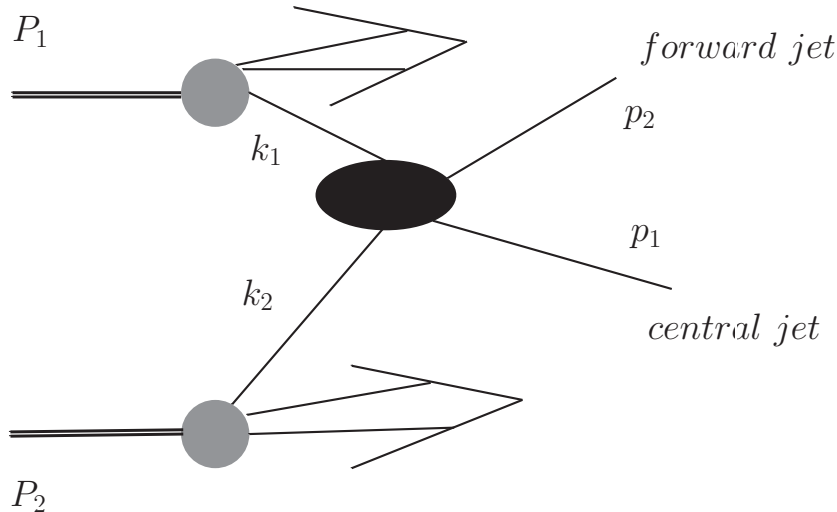


Figure 22: (Left) Jet production in the forward (assuming the proton moves toward positive rapidity) region in hadron-hadron collisions. (Right) Ratio of differential cross sections for central and forward dijet production at $\sqrt{s} = 5$ TeV as a function of the azimuthal distance between the jets, $\Delta\phi$, for pp and $p+Pb$ collisions with two different cuts on the jets p_T . Courtesy of Krzysztof Kutak.

Photons

Direct Photon Production in pQCD

Direct photon spectra for pp compared to $p+\text{Pb}$

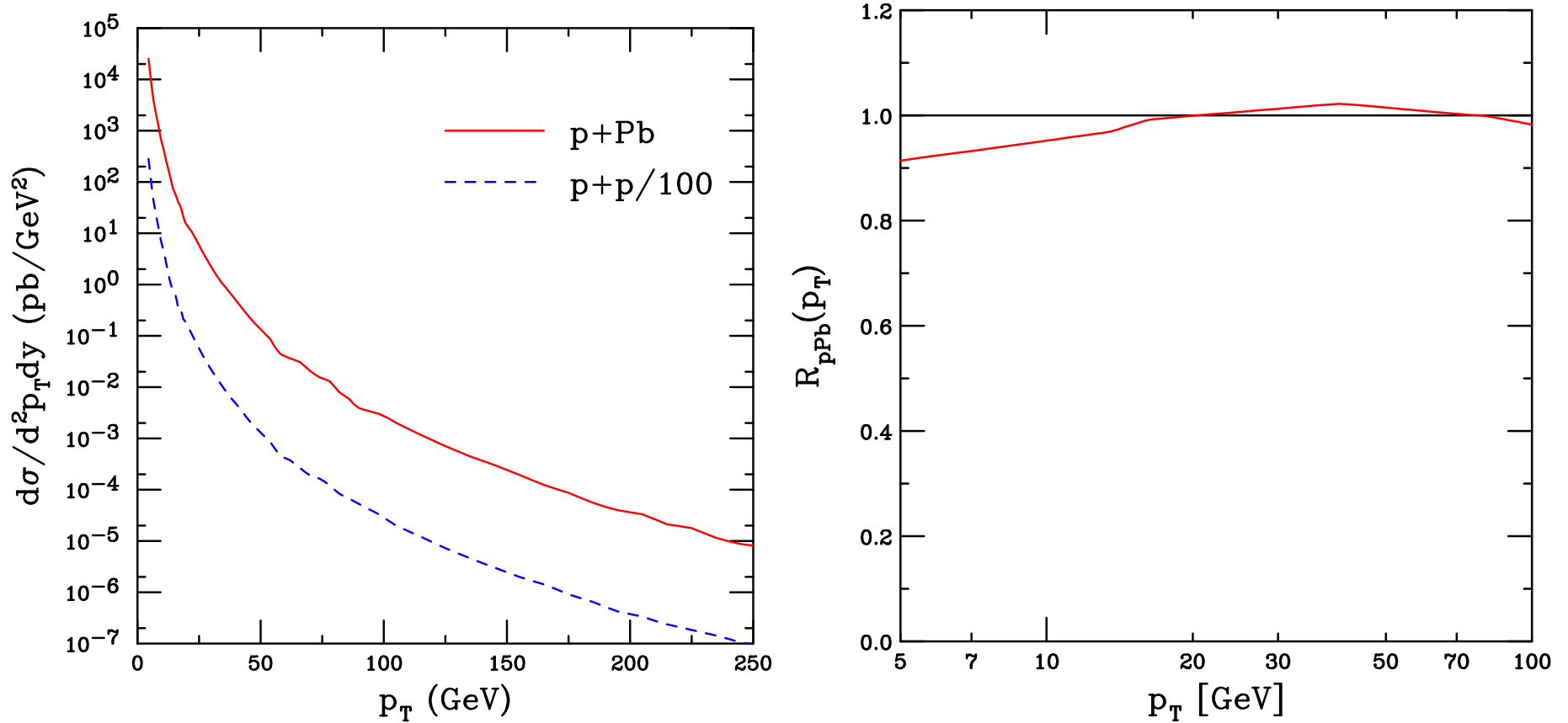


Figure 23: (Left) The direct photon p_T distribution at $y = 0$ in the lab frame. The $p+p$ distribution is scaled down by two orders of magnitude. The $p+\text{Pb}$ cross section is normalized to one proton-nucleon collision. An isolation cut of $E_T < 5$ GeV for hadronic energy within a $R = 0.4$ cone has been imposed. The spectra are shown in the laboratory frame of the collisions. In particular, in the lab frame the spectrum is for $y_{\text{lab}} = 0$ for pp and $y = 0.47$ (in the direction of the proton) for $p+\text{Pb}$. The calculations were performed employing jetphox (Catani *et al.*) with EPS09 for the parton densities. (Right) The corresponding modification factor $R_{p\text{Pb}}(p_T)$. Note the logarithmic p_T scale. Courtesy of R. Fries.

Enhanced Dijet and Photon+Jet Broadening

Transverse momentum imbalance, $\mathbf{q}_T = \mathbf{p}_{T_1} + \mathbf{p}_{T_2}$

Broadening quantified by difference $\Delta\langle q_T^2 \rangle = \langle q_T^2 \rangle_{hA} - \langle q_T^2 \rangle_{hp}$, double parton scattering from initial or final state, T^I and T^F are twist-4 correlation functions

$$\Delta\langle q_T^2 \rangle = \left(\frac{8\pi^2\alpha_s}{N_c^2 - 1} \right) \frac{\sum_{a,b} f_{a/p}(x') \left[T_{b/A}^{(I)}(x) H_{ab \rightarrow \gamma d}^I(\hat{s}, \hat{t}, \hat{u}) + T_{b/A}^{(F)}(x) H_{ab \rightarrow \gamma d}^F(\hat{s}, \hat{t}, \hat{u}) \right]}{\sum_{a,b} f_{a/p}(x') f_{b/A}(x) H_{ab \rightarrow \gamma d}^U(\hat{s}, \hat{t}, \hat{u})}$$

$$T_{q/A}^{(I)}(x) = \int \frac{dy^-}{2\pi} e^{ixp^+y^-} \int \frac{dy_1^- dy_2^-}{2\pi} \theta(y^- - y_1^-) \theta(-y_2^-) \frac{1}{2} \langle p_A | F_{\alpha^+}(y_2^-) \bar{\psi}_q(0) \gamma^+ \psi_q(y^-) F^{+\alpha}(y_1^-) | p_A \rangle$$

$$T_{g/A}^{(I)}(x) = \int \frac{dy^-}{2\pi} e^{ixp^+y^-} \int \frac{dy_1^- dy_2^-}{2\pi} \theta(y^- - y_1^-) \theta(-y_2^-) \frac{1}{xp^+} \langle p_A | F_{\alpha^+}(y_2^-) F^{\sigma+}(0) F_{\sigma}^+(y^-) F^{+\alpha}(y_1^-) | p_A \rangle$$

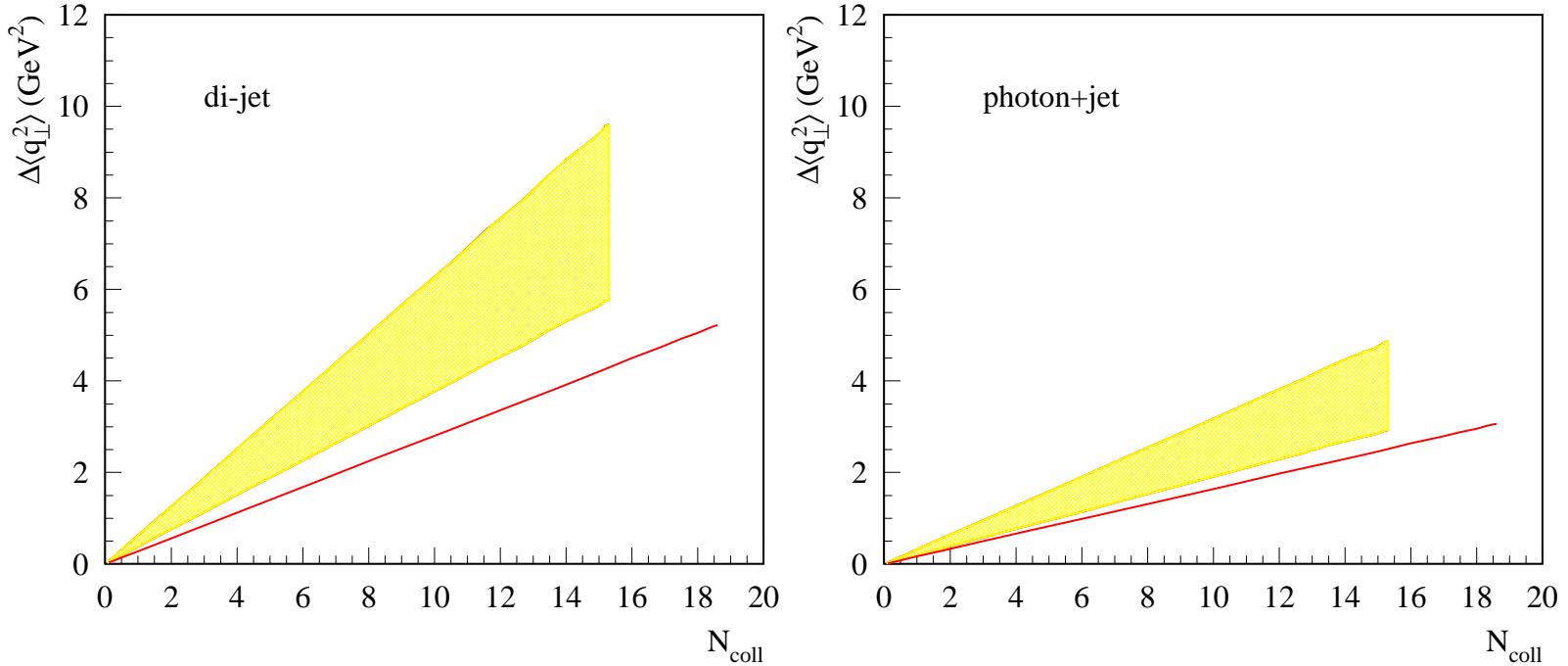


Figure 24: Nuclear broadening $\Delta\langle q_T^2 \rangle$ for dijet (left) and photon+jet (right) production in pA collisions as a function of N_{coll} . Fixed rapidity $y_1 = y_2 = 2$ is used for $\sqrt{s} = 5$ TeV LHC $p+\text{Pb}$ collisions with $y_1 = y_2 = 1$ for 200 GeV $d+\text{Au}$ collisions. At 5 TeV, the jet p_T integral is over $30 < p_T < 40$ GeV, while for RHIC, the range is $15 < p_T < 25$ GeV. The band shows a range of predictions in LHC kinematics while the red line is for RHIC. Courtesy of Ivan Vitev.

Results from the $p+\text{Pb}$ Test Run

ALICE $R_{p\text{Pb}}$ data uses pp reference obtained by interpolating between data at 2.76 and 7 TeV, R_{pA} is formed by comparing $|\eta_{\text{lab}}| < 0.8$ in $p+\text{Pb}$ to $-0.3 < \eta_{\text{cm}} < 1.3$; calculation of $\eta_{\text{cm}} = \eta_{\text{lab}} + 0.465$ is accurate for $m \sim 0$ or high p_T

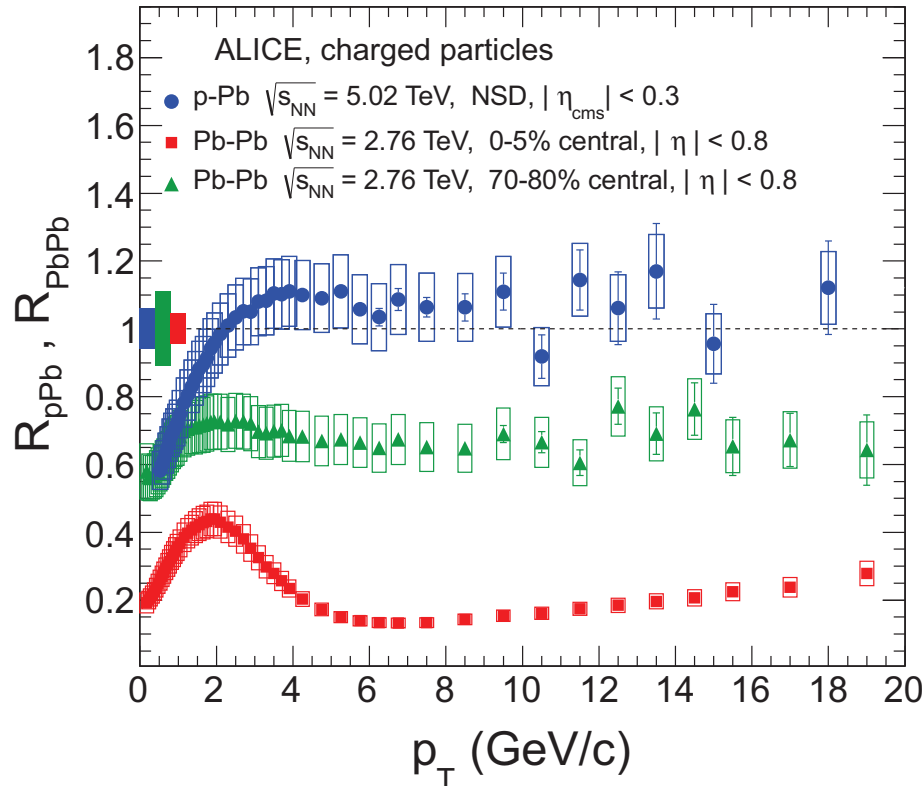


Figure 25: The minimum bias $R_{p\text{Pb}}$ ratio is compared to central and peripheral values of R_{AA} (left) and various models (right). From ALICE Collaboration, arXiv:1210.4520 [nucl-ex].

Gauge Bosons

Cold Matter Effects on W and Z Production

Isospin effects evident for W^+ and W^- production, small effect on Z

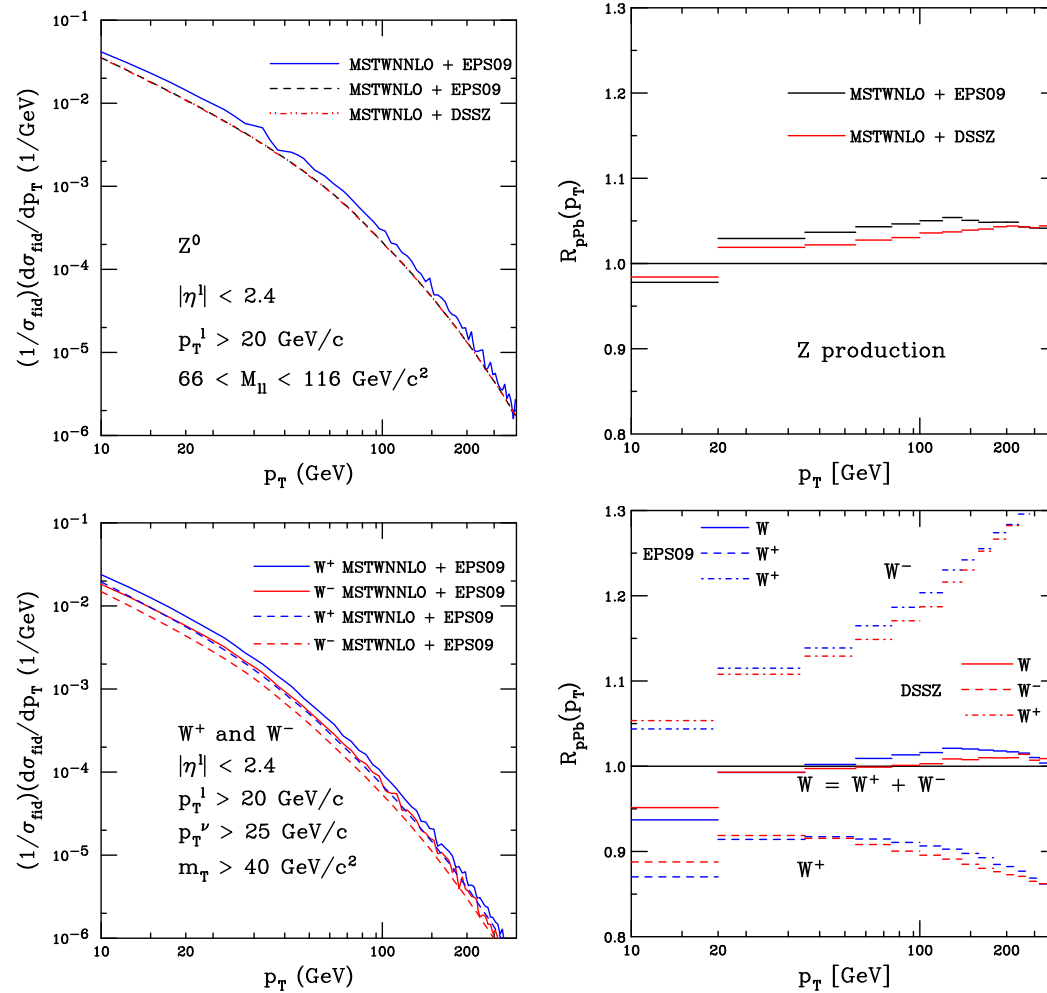


Figure 26: Normalized differential cross section (with ATLAS acceptance cuts on the leptons) $(1/\sigma_{\text{fid}})(d\sigma_{\text{fid}}/dp_T^Z)$ and R_{pPb} for Z (top) and W (bottom) boson production. In the case of W production, σ_{fid} is the sum $W = (W^+ + W^-)$ in the fiducial phase space and p_T^W is the transverse momentum of the W^+ or W^- . Courtesy of Zhang *et al.*

Differences in W Charge Asymmetry in pp and $p+Pb$

Significant difference in W^+ and W^- rapidity distributions due to $p+Pb$ vs pp
 Little difference whether calculation is NLO or NNLO

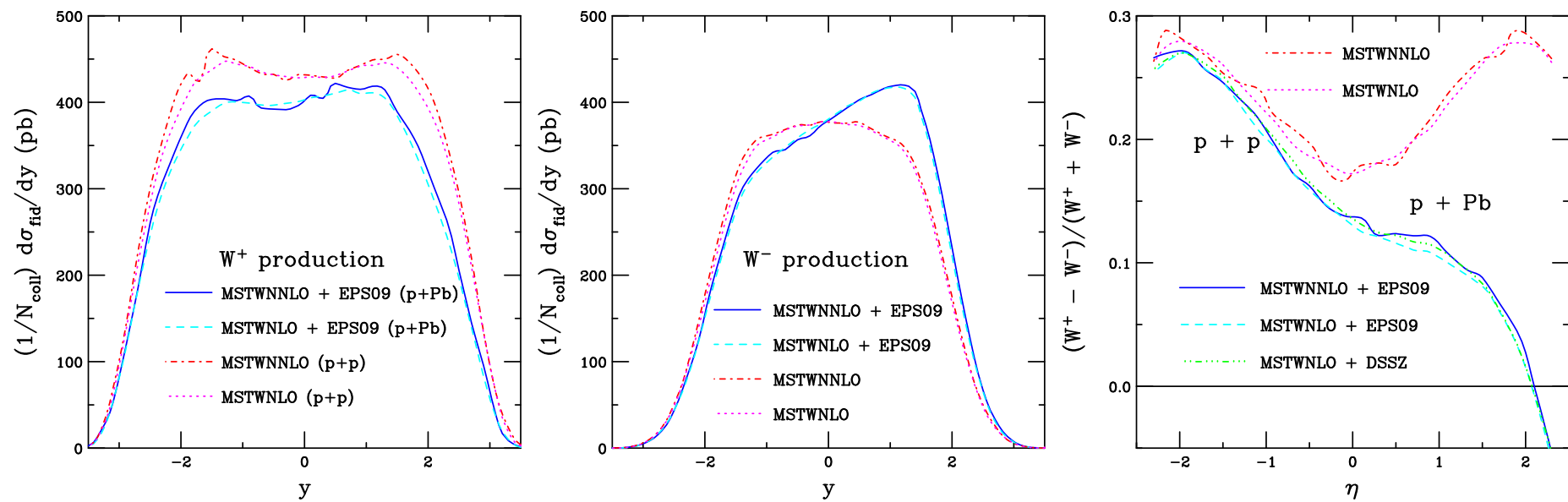


Figure 27: The W^+ (left) and W^- (center) rapidity distributions. (Right) The charge asymmetry $(N_{W^+} - N_{W^-})/(N_{W^+} + N_{W^-})$ as a function of the charged lepton pseudorapidity for W boson productions in both $p+p$ and $p+Pb$ collisions at 5 TeV. Courtesy of Zhang *et al.*

Broadening of Vector Boson Production

Quarkonium broadening much larger than W and Z broadening

$$\Delta\langle q_T^2 \rangle_{\text{HQ}}^{\text{CEM}} = \left(\frac{8\pi^2\alpha_s}{N_c^2 - 1} \lambda^2 A^{1/3} \right) \frac{(C_F + C_A)\sigma_{q\bar{q}} + 2C_A\sigma_{gg} + \Delta\sigma_{gg}}{\sigma_{q\bar{q}} + \sigma_{gg}} \approx 2C_A \left(\frac{8\pi^2\alpha_s}{N_c^2 - 1} \lambda^2 A^{1/3} \right)$$

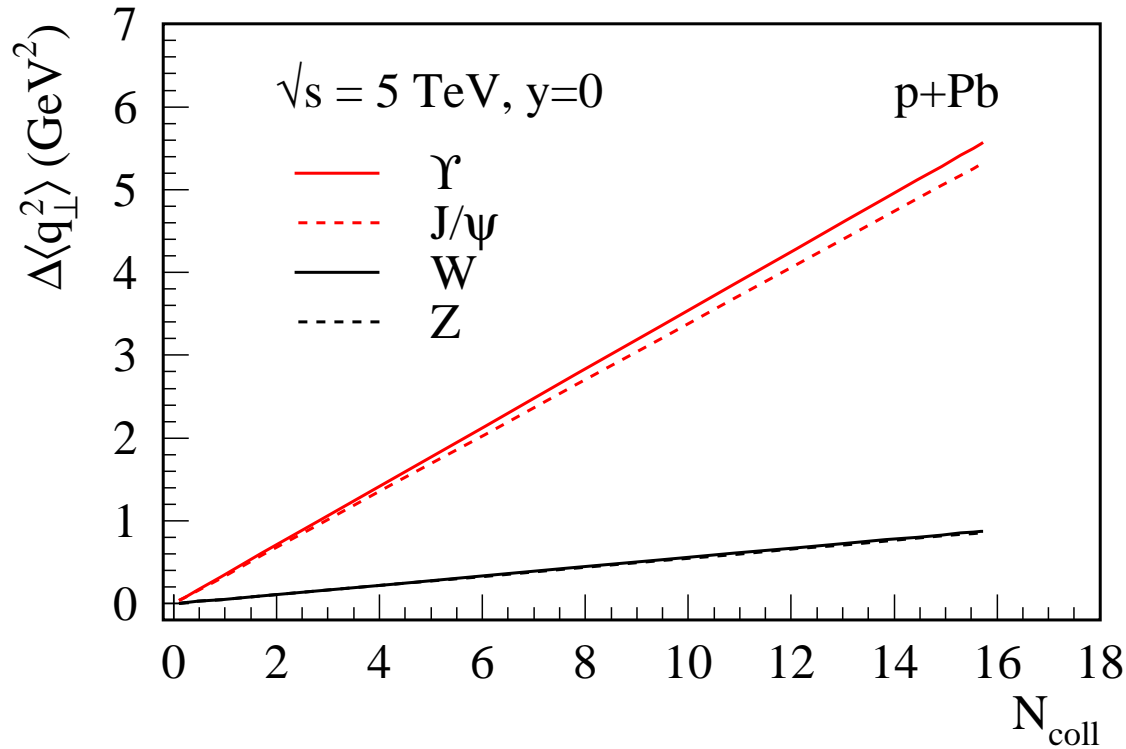


Figure 28: The transverse momentum broadening of vector boson production in $p+\text{Pb}$ collisions at $y = 0$, shown as a function of N_{coll} . The Υ (red solid), J/ψ (red dashed), W^\pm (black solid), and Z^0 (black dashed) results are given. Courtesy of Qiu *et al.*